

## Modeling the Tilt of Bend-Traversing Turbidity Currents: Implications for Sinuous Submarine Channel Development



### Key Points:

- We present a novel methodology to assess the contested controlling factors on the development of sinuous channels
- Deep and dense flows that pass through small channels in steep slopes, regardless of the latitude, promote sinuosity
- Dilute and shallow flows that pass through large channels in low gradient systems hinder sinuosity development at any latitude

### Correspondence to:

A. D. McArthur,  
[a.mcarthur@leeds.ac.uk](mailto:a.mcarthur@leeds.ac.uk)

### Citation:

Crisóstomo-Figueroa, A., Dorrell, R. M., Amy, L., McArthur, A. D., & McCaffrey, W. D. (2024). Modeling the tilt of bend-traversing turbidity currents: Implications for sinuous submarine channel development. *Journal of Geophysical Research: Oceans*, 129, e2023JC020131. <https://doi.org/10.1029/2023JC020131>

Received 23 JUN 2023  
 Accepted 16 SEP 2024

### Author Contributions:

**Conceptualization:** Adriana Crisóstomo-Figueroa, Robert M. Dorrell, Lawrence Amy, Adam D. McArthur, William D. McCaffrey

**Data curation:** Adriana Crisóstomo-Figueroa

**Formal analysis:** Adriana Crisóstomo-Figueroa, Robert M. Dorrell, Lawrence Amy, Adam D. McArthur




**Funding acquisition:** Adam D. McArthur, William D. McCaffrey

**Investigation:** Adriana Crisóstomo-Figueroa

**Methodology:** Adriana Crisóstomo-Figueroa, Robert M. Dorrell, Lawrence Amy, Adam D. McArthur

**Project administration:** Adam D. McArthur, William D. McCaffrey

**Resources:** Adam D. McArthur

Adriana Crisóstomo-Figueroa<sup>1</sup> , Robert M. Dorrell<sup>2</sup> , Lawrence Amy<sup>3</sup>, Adam D. McArthur<sup>1</sup> , and William D. McCaffrey<sup>1</sup>

<sup>1</sup>Institute of Applied Geosciences, University of Leeds, Leeds, UK, <sup>2</sup>Energy and Environment Institute, University of Hull, Hull, UK, <sup>3</sup>School of Earth Sciences, University College Dublin, Belfield, Ireland

**Abstract** The controls on the development of submarine channel sinuosity are contested: slope gradient and Coriolis forcing have both been recognized as key governing factors: gradient via an inverse relationship (low sinuosity at high slope and vice versa), and Coriolis forcing through its effect on sedimentation patterns (reducing lateral bend migration, and hence sinuosity development, at high latitudes and/or in large channels). Using theoretical models to calculate the bulk properties of channelized turbidity currents, this study investigates the joint role of the Coriolis force and parameters including channel size, downchannel slope and turbidity current properties in the development of submarine channel sinuosity. Model validation is undertaken through the comparison of the calculated turbidity current tilting against the measured tilting of channel levees in the Northwest Atlantic Mid-Ocean Channel; this approach is then used to evaluate the controls on channel sinuosity in nine other modern seafloor channels. The results indicate that the Coriolis force only becomes significant when the size of the channel, the slope gradient and flow conditions are within appropriate ranges instead of solely being dependent on latitude. Thus, thick and dense ( $\geq 1\%$  bulk sediment concentration) flows traveling within steep-gradient, small-scale channels were shown to be relatively less susceptible to flow modification by Coriolis forcing even at high latitudes. On the other hand, thin and dilute ( $\ll 1\%$  bulk sediment concentration) flows in shallow-gradient, large-scale channels showed susceptibility to Coriolis forcing at all latitudes. These results offer new insights into submarine channel evolution and intra-channel sedimentation patterns.

**Plain Language Summary** Sediments are widely distributed in the oceans by underwater currents akin to powder snow avalanches. These “turbidity currents” may sculpt the sea floor to build submarine channels which, like rivers, may range in sinuosity from being virtually straight to highly sinuous. Several competing controls have been suggested to explain this variation. Some argue that slope is most important, with low sinuosity channels forming on high angle slopes and vice versa. Others claim that the Coriolis force, which affects flows moving across a rotating surface (such as the Earth), is the main control - either via latitude alone (with high sinuosity channels restricted to lower latitudes) or only affecting channels that are large enough. To test these ideas we developed a new numerical modeling approach that looks at the combined effects of channel axis gradient, channel size and flow conditions. By modeling the tilt of turbidity currents flowing around bends we show that single factors cannot be used to explain channel sinuosity. The model is tested with real world data. Although sinuosity is generally greater at low latitudes there are exceptions; variations across a range of controlling factors can produce channels of any sinuosity at any latitude.

## 1. Introduction

Turbidity currents are a type of subaqueous flow that are driven by their excess density compared to the ambient fluid owing to the presence of suspended sediment (Talling et al., 2012). They can travel thousands of kilometers from shallow to deepwater settings and build channels that facilitate the transport of sediment (Piper & Normark, 2001), organic carbon (Hage et al., 2020) and pollutants (Zhong & Peng, 2021) (Figure 1). Furthermore, turbidity currents may damage seafloor infrastructure such as pipelines and communication cables (Clare et al., 2020; Khripounoff et al., 2003).

During their passage through submarine slopes and across basin floors, turbidity currents commonly construct channels. Submarine channels can develop sinuous planform morphologies, building deposits with complex architectural geometries (Peakall et al., 2007; Wynn et al., 2007); their reservoir potential makes channels of

© 2024. The Author(s).

This is an open access article under the terms of the [Creative Commons Attribution License](https://creativecommons.org/licenses/by/4.0/), which permits use, distribution and reproduction in any medium, provided the original work is properly cited.

Attribution License, which permits use, distribution and reproduction in any medium, provided the original work is properly cited.

**Supervision:** Robert M. Dorrell, Lawrence Amy, Adam D. McArthur, William D. McCaffrey  
**Validation:** Adriana Crisóstomo-Figueroa, Robert M. Dorrell, Lawrence Amy  
**Visualization:** Adriana Crisóstomo-Figueroa, Robert M. Dorrell  
**Writing – original draft:** Adriana Crisóstomo-Figueroa, Adam D. McArthur  
**Writing – review & editing:** Adriana Crisóstomo-Figueroa, Robert M. Dorrell, Lawrence Amy, William D. McCaffrey

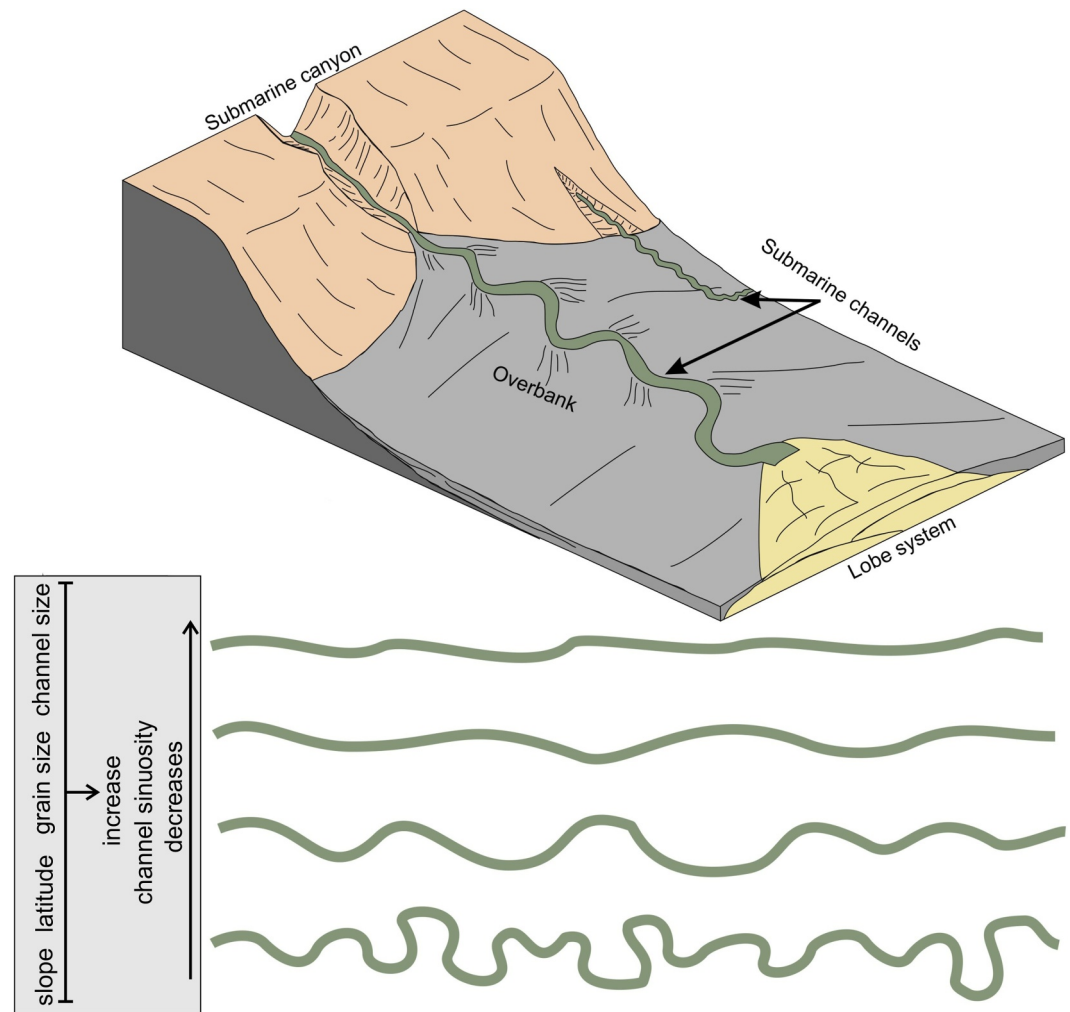


**Figure 1.** Schematic diagram of submarine channels on the slope and basin plain (adapted from Wells & Cossu, 2013) and proposed controls on the development of sinuosity in submarine channels (see text).

interest for hydrocarbon exploration (Abreu et al., 2003; Mayall et al., 2006) and for CO<sub>2</sub> storage (Marshall et al., 2016).

The sedimentological and hydraulic factors controlling the development of submarine channel sinuosity have been a subject of debate (Clark et al., 1992; Kane & McCaffrey, 2008; Peakall et al., 2000, 2012, 2013; Sylvester & Pirmez, 2019; Wynn et al., 2007). Steep downchannel slope gradients and coarse-grained systems have been linked to the development of low sinuosity channels, with shallow gradients and fine-grained systems linked to the development of high sinuosity channels (Clark et al., 1992) (Figure 1). However, through the analysis of peak sinuosities from channels across the globe, Peakall et al. (2012) suggested that the peak sinuosity-slope gradient relationship was statistically weak, whereas the sinuosity-latitude relationship showed a stronger correlation. They proposed that this relationship might be controlled by the Coriolis force and variations in flow and sediment type with latitude. Furthermore, experimental work in rotating flumes has been interpreted to support the hypothesis that Coriolis forcing can impact turbidity current structure so as to hinder sinuosity development, indicating that the latitudinal position of channels should be a strong control on the development of sinuosity (Cossu et al., 2010; Cossu & Wells, 2010; Davarpanah Jazi et al., 2020; Wells & Cossu, 2013). Consequently, low sinuosity channels are thought to be characteristic of high latitude areas where Coriolis forces are stronger (e.g., the Northwest Atlantic Mid-Ocean Channel (NAMOC), Klaucke et al., 1997), whereas high sinuosity channels have been related to low latitudes and scale where Coriolis forces are reduced (e.g., the Amazon Channel (Pirmez & Imran, 2003). However, based on the analysis of ancient turbidite channel systems of the Cerro Toro

Formation in Chile, Cossu et al. (2015) suggested that smaller channels (i.e., with widths in the orders of tens and hundreds of meters) were less influenced by the Coriolis force. Imran et al. (1999) suggested that both latitude and scale are key factors controlling whether the Coriolis force dominates using numerical modeling of turbidity currents in the NAMOC and Amazon channels.

Laboratory experiments have shown that the Coriolis force can modify the three-dimensional structure of turbidity currents, including the flow–ambient fluid interface (i.e., the upper fluid interface); around bends the tilt of the interface depends on the interplay between Coriolis and centrifugal forces (Cossu & Wells, 2013; Wells & Dorrell, 2021). A key parameter used to evaluate whether Coriolis or centrifugal forces dominate is the Rossby number ( $Ro$ ). Thus, under weak northern hemisphere rotation ( $Ro \gg 1$ ) where Coriolis forcing is low, the balance between pressure and centrifugal forces predominates, resulting in an interface that changes its tilt direction around successive bends, such that the interface always tilts toward the inner bank (Figure 2a) (Cossu & Wells, 2010; Davarpanah Jazi et al., 2020). The velocity maximum and high-density region of the flow are co-located toward the outer bank in this scenario (Davarpanah Jazi et al., 2020) and therefore alternate channel sides between successive bends, which promotes bend expansion and sinuosity development (Straub et al., 2008; M. G. Wells & Cossu, 2013). Flow superelevation and overspill results in cross-sectional levee asymmetry, with outer bend levee crests being higher (Straub & Mohrig, 2008).

Under strong northern hemisphere rotation ( $Ro \sim 1$ ) (Figure 2b), the tilt of anticlockwise flows also tilts toward the inner bank and tilt superelevation arises due to the effect of a stronger Coriolis force (Cossu & Wells, 2010; Wells & Cossu, 2013). In clockwise flows, however, the Coriolis force deflects the bulk of the flow and causes a force balance rearrangement so that the Centrifugal and pressure forces oppose the Coriolis force (Figure 2b). Therefore, the flow interface is reversed and tilts toward the outer bank (Figure 2b) (Cossu & Wells, 2013). Furthermore, the velocity maximum is deflected toward the inner bend and the density core has been observed to be decoupled from the velocity field and remain directed toward the outer bend; this structure has been interpreted to diminish the potential for channels to develop sinuous bends, as there would be greater potential for erosion on the inner bend (Cossu & Wells, 2013; Davarpanah Jazi et al., 2020) and deposition on the outer bend where the maximum density is located (Davarpanah Jazi et al., 2020). Flow superelevation and overspill results in strong cross-sectional levee asymmetry, with the right levee always being higher when looking in a downstream direction in northern hemisphere scenarios (Figure 2b) (Cossu & Wells, 2013; Dorrell et al., 2013). The opposite force balances apply in the southern hemisphere, leading to higher left levees looking downstream.

The role of Coriolis forces in channel sinuosity development was re-evaluated by Sylvester et al. (2013) and Sylvester and Pirmez (2019) who showed that high sinuosity channels are not exclusive to low latitude areas (e.g., the Danube Channel (Popescu et al., 2004) and that low sinuosity channels may also occur at low latitudes (e.g., the Tanzania Channel Bourget et al., 2008). Using a large data set of meander bends from channels across the globe, they showed that the latitude does not correlate well with sinuosity (i.e., contrary to the findings from Peakall et al. (2012) using only the peak sinuosities). They suggested that the Coriolis force was unlikely to have a big impact on the development of sinuosity in submarine channels and that it might only play a role in large scale channels at high latitude systems, such as the NAMOC.

In the work described here the slope of the upper fluid interface tilting was calculated using the surface slope equation of Komar (1969) that describes the force balance of centrifugal, Coriolis and pressure forces, combined with the model of Parker et al. (1987) to account for the gravitational driving force and drag. Channel morphometric data from the NAMOC were extracted from the literature (Klaucke et al., 1997) and were used to test whether the combined modeling technique could be used with confidence to calculate cases of deflection of the upper fluid interface tilt due to Coriolis forces. Hence, the aims of this work are as follows.

1. To contribute to the debate on whether Coriolis forces control the development of sinuosity in submarine channels. If tilt modification is linked to the deflection of the velocity and density maxima within flows, promoting changes in erosion and deposition patterns (Davarpanah Jazi et al., 2020), it may consequently hinder the development of channel sinuosity, as experimental observations suggest (Cossu & Wells, 2010; Davarpanah Jazi et al., 2020; Wells & Cossu, 2013).
2. To conduct a parametric study to assess the joint influence of parameters including latitude, radius of curvature, downchannel slope and depth-averaged flow properties on modifying the upper fluid interface. A modeling approach entailing the solution of both cross- and downchannel forces enables a broader set of

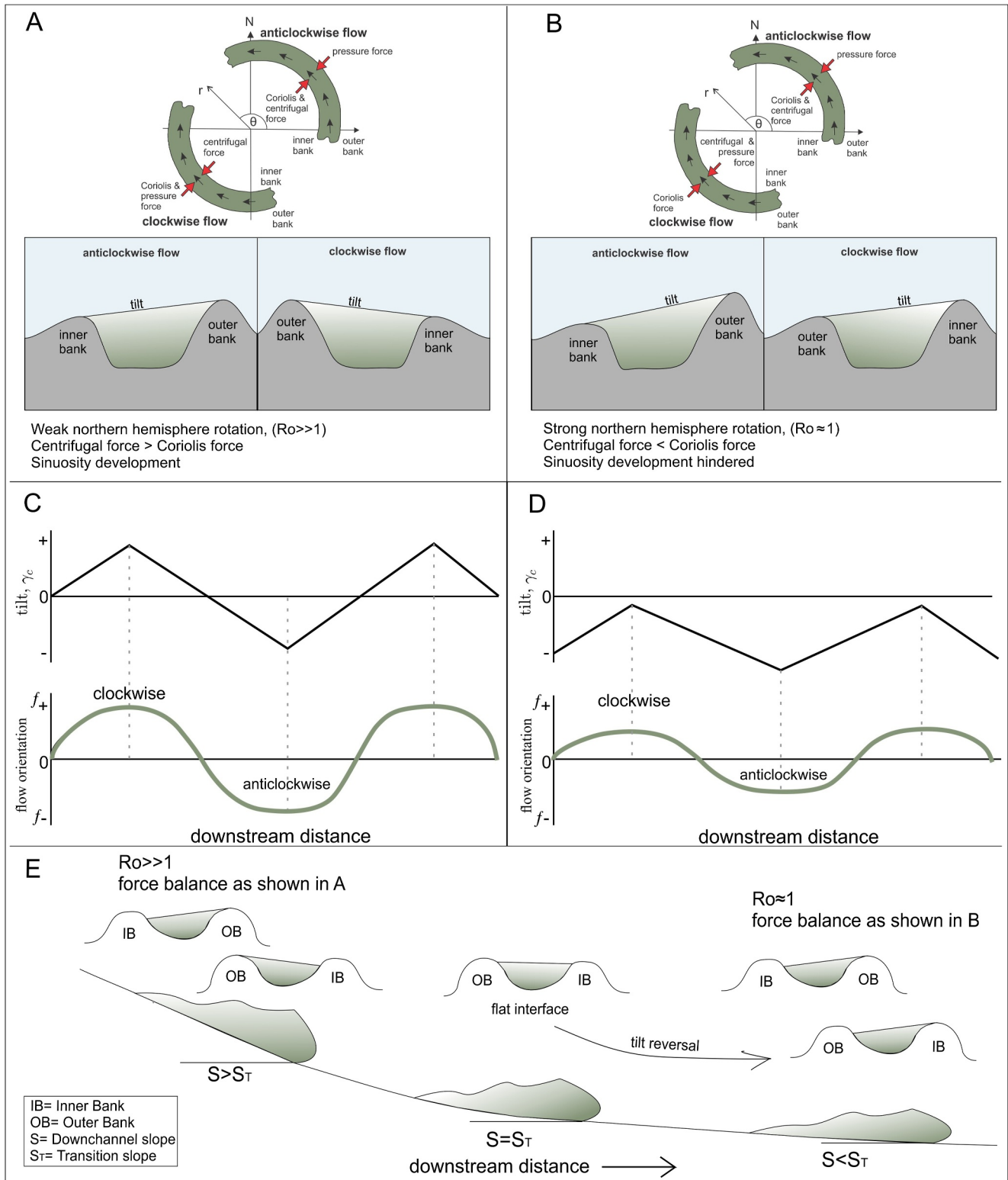


**Figure 2.** Force balance and tilting under (a) weak northern hemisphere rotation and (b) strong northern hemisphere rotation (adapted from Dorrell et al. (2013)); cross-sections looking in the downstream direction (c) and (d) show a saw-tooth pattern representing the response of the calculation of the tilt, and its theoretical channel form with a constant geometry downstream.  $f$  is the Coriolis acceleration which is positive for clockwise flows and negative for anticlockwise flows. (e) Sketch of the change in the upper interface of the current when the downchannel slope is less, equal or greater than the Transition Slope (See Results).

- parameters to be evaluated than experimental work can cover, better identifying the conditions that may affect sinuosity development.
- To determine whether the described modeling approach and any new findings arising can be applied more generally, to assess their likelihood of other channelized systems developing straight versus sinuous geometries.

## 2. Methods

### 2.1. Estimating the Upper Fluid Interface Tilt

The slope of the tilted upper fluid interface was approximated through the surface-slope equation, which describes the momentum balance of the pressure gradient force, the Coriolis force and the centrifugal force across a channel assuming depth averaged, bankfull conditions (Equation 1) where currents exactly fill the channel confinement (Komar, 1969)

$$g\delta C\gamma_c = \pm fU + \frac{U^2}{r}, \quad (1)$$

where  $g = 9.81 \text{ m/s}^2$  gravity;  $\delta = (\rho_s/\rho_f - 1)$  is the submerged specific gravity (where  $\rho_s = 2,650 \text{ kg/m}^3$  is the density of quartz for the material in suspension, and  $\rho_f = 1,000 \text{ kg/m}^3$  is the density of the fluid);  $C$ , the bulk sediment concentration (vol./vol.);  $\gamma_c$  = the slope of the upper fluid interface (tilt) (m/m);  $f$  the Coriolis acceleration  $f = 2\Omega\sin\theta$ , where  $-f$  applies for clockwise flows and  $+f$  for anticlockwise flows (Figures 2c and d),  $\Omega$  is the Earth's rotation rate, and  $\theta$  the latitude;  $U$ , the downstream flow velocity in m/s; and  $r$ , the thalweg radius of curvature (m).

Equation 1 can be rewritten in terms of the densimetric Froude number,  $Fr$ , (Wells & Dorrell, 2021) where  $Fr = U/\sqrt{g\delta\bar{C}\bar{H}}$  (Parker et al., 1987),

$$\gamma_c = Fr^2 \left( \frac{\pm f\bar{H}}{Fr\sqrt{g\delta\bar{C}\bar{H}}} + \frac{\bar{H}}{r} \right), \quad (2)$$

where  $\bar{H}$  is the average flow depth (m).

Downchannel forces can be calculated using the balance of gravitational driving force with frictional drag at the bed, and through the entrainment of ambient water following the model of Parker et al. (1987) (e.g., Abad et al., 2011),

$$S = \frac{C_d + e_w \left(1 + \frac{Ri}{2}\right)}{Ri}, \quad (3)$$

where  $S$  is the downchannel slope in m/m;  $C_d = 0.0025$  (Abad et al., 2011; Konsoer et al., 2013), the drag coefficient that, for simplicity, is considered constant in all calculations;  $Ri$ , the bulk Richardson number, which scales inversely with  $Fr^2$  (Wells & Dorrell, 2021), is a measure of mixing of the upper fluid interface (Abad et al., 2011; Parker et al., 1987),

$$Ri = \frac{g\delta\bar{C}\bar{H}}{U^2} = \frac{1}{Fr^2}, \quad (4)$$

and  $e_w$ , the ambient water entrainment by mixing is defined using

$$e_w = \frac{0.00153}{0.0204 + Ri}, \quad (5)$$

a relation derived empirically by Parker et al. (1987) for turbidity currents.



The nonlinear least squares MATLAB solver (*lsqnonlin*) with the trust-region-reflective algorithm (Coleman & Li, 1996) was used with a tolerance point of  $10^{-12}$  to find optimal solutions of the upper fluid interface slope (tilt),  $\gamma_c$  (Equation 2), and the Froude number,  $Fr$  (Equation 3), to jointly solve for cross-channel forces (Komar, 1969) and downchannel forces, respectively (Abad et al., 2011). The solver represents an optimization technique that runs successive iterations to find the solutions that best fit the input parameters and set of equations given (i.e., Equations 2–5) with the minimum error (Dennis, 1977).

The degree to which turbidity currents are influenced by Coriolis forces can be determined by the dimensionless Rossby number (Wells & Dorrell, 2021)

$$Ro_R = \frac{U}{Lf}, \quad (6)$$

where  $L$  represents the horizontal length scale of the current, here  $L = r$ . The Rossby number can also be calculated as  $Ro_W = U/Wf$ , where  $W$  represents the channel width (Wells & Cossu, 2013).

In this study,  $r$  has been selected as the appropriate length scale for our calculations. Here,  $r$  represents the centrifugal force; then, when  $Ro_R = 1$ , centrifugal forces balance Coriolis forces (Wells & Dorrell, 2021). The successful mathematical application of the radius of curvature as the horizontal length scale has been demonstrated in several studies modeling the response of turbidity currents to Coriolis forces in sinuous channels.  $Ro_R$  has shown to accurately describe the balance of Centrifugal and Coriolis forces under experimental currents (e.g., Cossu et al., 2015; Cossu & Wells, 2010; Cossu & Wells, 2013; Davarpanah Jazi et al., 2020), theoretical currents (e.g., Sylvester & Pirmez, 2019) and field observations (e.g., Wells & Cossu, 2013).

Values of  $Ro_R \gg 1$  describe a centrifugal dominated flow, while  $Ro_R \approx 1$  describe flows where the Coriolis force dominates (Cossu & Wells, 2010; Wells & Dorrell, 2021).

## 2.2. Validating Model Tilt Predictions With Inferred Tilting in the NAMOC

The NAMOC is a large-scale, low sinuosity channel located in the Labrador Sea that displays a strong channel-levee asymmetry (Figure 3a) (Klaucke et al., 1997, 1998). The right-hand levee is consistently higher than the left levee despite changes in bend orientation, which has been attributed to the effect of Coriolis causing flow deflection and preferential overspill to the right-hand bank (Klaucke et al., 1997). Therefore, this channel constitutes a good field example to test the accuracy of the computed model predictions of the ambient-fluid interface slope  $\gamma_c$  to the observed tilting of the channel-levees,  $\gamma_m$  (assuming that the observed levee asymmetry is a proxy for the tilting of the flows traveling through the channel). Furthermore, morphometric measurements from the channel were analyzed to evaluate the influence of the radius of curvature, downchannel slope and latitude on the observed changes in the tilt and sinuosity.

Channel bend morphometrics were obtained from Klaucke (1995) and Klaucke et al. (1997), which cover a  $\sim 950$  km long stretch of the channel, ranging in latitude from  $60^\circ$  to  $53^\circ$ . Channel bend data ( $H, S, \theta$  and  $r$ ) were used as input parameters in Equations 2 and 3 to calculate  $\gamma_c$ ; while the channel-levee tilt was calculated through  $\gamma_m = \Delta H/w$ . Two data points from clockwise bends were omitted from the analysis due to documented levee collapses (red arrows in Figure 3b) (Klaucke et al., 1997). Levee collapses increase  $\Delta H$ , thus making  $\gamma_m$  larger than the tilting expected from the effect of overspilling currents, invalidating comparisons of  $\gamma_c$  and  $\gamma_m$ .

Input values of  $C$  were estimated through

$$C = \frac{1}{\delta} \left( \frac{\rho_t}{\rho_f} - 1 \right), \quad (7)$$

where  $\rho_t$  is the current density (Konsoer et al., 2013). Klaucke et al. (1997) calculated that excess densities  $\rho_t - \rho_f$  in the NAMOC ranged from 1 to  $12 \text{ kgm}^{-3}$  which, using Equation 7, are equivalent to  $C$  of 0.06%–0.7%, respectively. Furthermore, a third value between the low and high  $C$  values was considered, where  $C = 0.2\%$ .

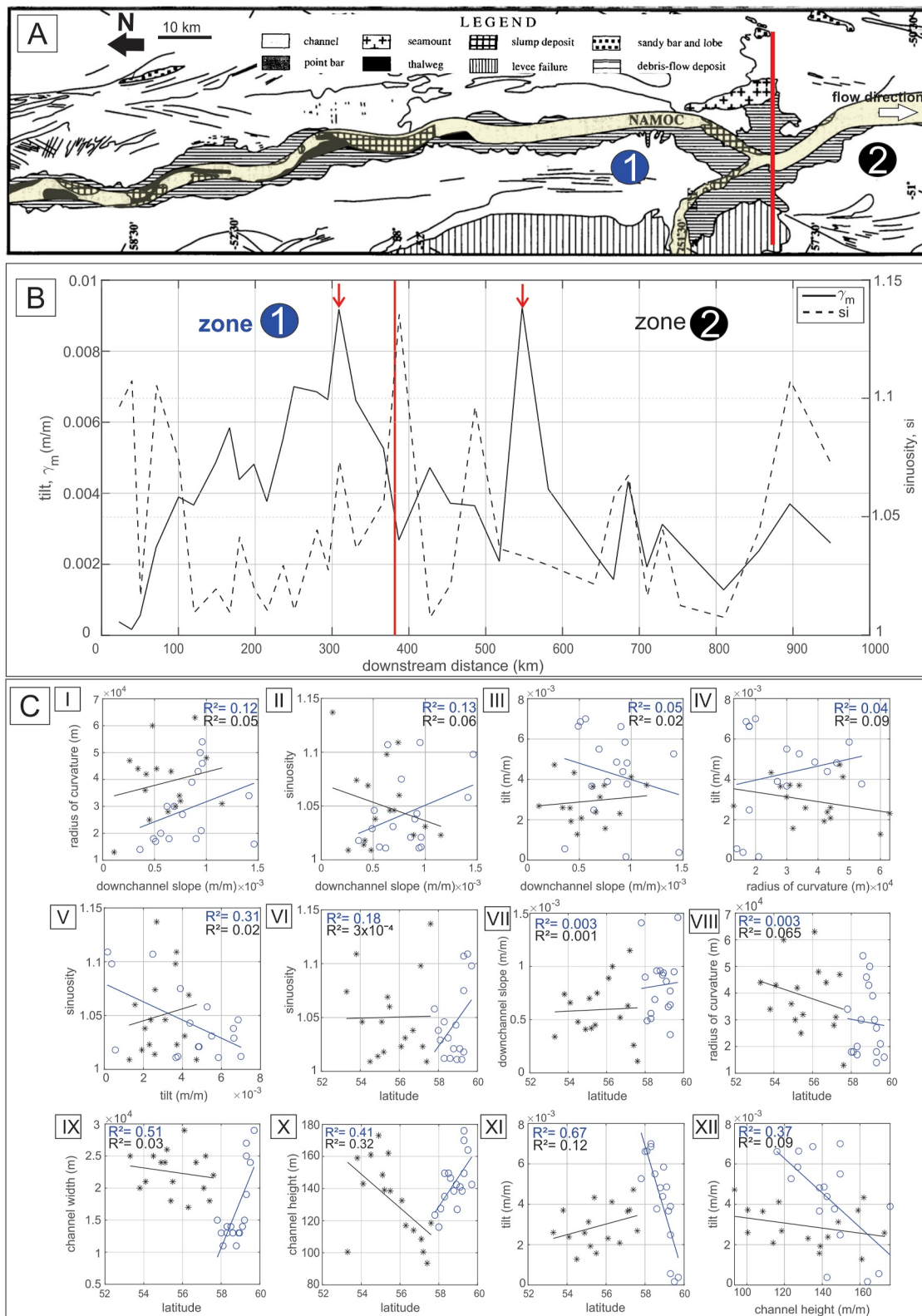


**Figure 3.** NAMOC map and morphometrics extracted from Klaucke et al. (1997) (a) Geological sketch of the NAMOC showing its division and low sinuosity platform (adapted from Klaucke et al., 1997). (b) Downchannel changes in the measured tilt and sinuosity. Zone 1 corresponds to the ‘equilibrium channel’ whereas zone 2 to the ‘modified equilibrium channel’. Red arrows indicate locations of levee collapse. (c) Morphometric relationships for each channel zone with calculated  $R^2$  values. Blue circles correspond to data points from zone 1 and black asterisks to zone 2.

**Table 1**

Input Parameters Used in the Modeling of the Upper Interface Tilting for Low ( $C = 0.02\%$ ), Medium ( $C = 0.2\%$ ) and High ( $C = 2\%$ ) Sediment Concentration Groups

$r$ (m)	Latitude $\theta$ ( $^\circ$ )	$H$ (m)	$S$ (m/m)
500	5	10–200	$10^{-3}$ – $10^{-1}$
3,000			
30,000			
500	35		
3,000			
30,000			
500	55 $^\circ$		
3,000			
30,000			

### 2.3. Calculating Changes in the Upper Interface Tilting Due to Hydraulic, Morphological and Latitudinal Changes

A coordinate-normal system was used to calculate the changes in the upper interface tilting  $\gamma_c$ , where  $\gamma_c$  values derived from clockwise flows retain their positive sign (Figure 2c), whereas  $\gamma_c$  values derived from anticlockwise flows were multiplied by  $-1$  to represent the change in tilt direction (Figures 2a and 2c), hence producing a saw-tooth pattern with positive peaks and negative troughs that indicates that the interface tilts normally toward the inner bank (Figures 2a and 2c). Therefore, when the calculation derives only negative peaks (Figure 2d), it is interpreted that the tilt  $\gamma_c$  is reversed in clockwise flows (Figure 2b) due to Coriolis (for a northern hemisphere case). The theoretical channel form used with a constant geometry downstream is also shown in Figures 2c and 2d. The ratio  $\gamma_r$  is a measure of the tilting magnitude change between consecutive bends.

Equations 2–5 were used to evaluate the degree to which changes in the Coriolis force, the turbidity current properties and the confining channel morphology impact changes in  $\gamma_c$ . Three modeling groups for low ( $C = 0.02\%$ ), medium ( $C = 0.2\%$ ) and high ( $C = 2\%$ ) sediment concentration flows were evaluated for turbidity currents traveling through a channel with a decreasing downchannel slope ( $10^{-1}$ – $10^{-3}$  m/m) and a flow depth that decreases with distance (200–210 m) (Table 1). For each group, three fixed latitudes ( $5^\circ$ ,  $35^\circ$  and  $55^\circ$ ), which are representative of channels located at low, mid and high latitudes, were chosen to evaluate the latitudinal effect and three fixed radii of curvature (500 m, 3,000 m and 30,000 m) were used to evaluate the effect of changes in the scale of the bend.

### 2.4. Calculating the Downchannel Transition Slope

Assuming that a flat upper interface represents the point of transition to lateral interface deflection due to Coriolis forcing (e.g., Figure 2e), then  $\gamma_c = 0$  in Equation 2 and  $Ro_r = -1$  (Wells & Dorrell, 2021). Therefore, the downchannel slope  $S_T$  at which the transition occurs was approximated through Equation 3 and

$$Fr\sqrt{g\delta CH} = -fr, \quad (8)$$

where  $Fr$  values were used as inputs into Equation 3 through the relationship established in Equation 4 (Wells & Dorrell, 2021). Hence,  $S_T$  defines the minimum (threshold) downchannel slope needed in a channel for the development of sinuosity.  $\gamma_c$ ,  $Fr$  and  $S_T$  are solved locally at each bend and are dependent of the given bend morphometrics and instantaneous flow conditions, hence, the solutions at a downstream bend are independent of the solutions in its preceding bend.

The calculation of  $S_T$  allows the evaluation of the conditions that promote a reversed tilting over a wider range of latitudes, radius of curvature and flow conditions compared to those used in Section 2.3. The *meshgrid* function in MATLAB was used to create three 2-D grids with vectors  $x$  and  $y$  to calculate contour plots of  $S_T$  and assess its variation as a function of  $r$ ,  $C$ ,  $H$ , and latitude  $\theta$ . The range of  $r$  values shown in Table 2 was used as input in vector  $x$  for all the grids whereas vector  $y$  took the range of values from  $C$ ,  $H$  and  $\theta$  (Table 2) in the first, second and third grid, respectively. The number of datapoints in each vector was determined by a length,  $z$ , where  $z = 300$ . Each 2-D grid produced was used as input into Equation 8 together with the baseline values for each parameter when not varied within the grid (Table 2).

**Table 2**

Input Parameters in the Calculation of the Tilting Transition Slope

	$r$ (m)	$C$ (%)	$H$ (m)	Latitude $\theta$ ( $^\circ$ )
Range	90–65,000	0.01–1	5–300	3–90
Baseline value	–	0.2	100	35

Contours of  $S_T$  as a function of latitude and radius for different flow properties were produced and submarine channel data available from nine channels (i.e., Amazon, Danube, Knight Inlet, Monterey, NAMOC, Nile, Rhone, Tanzania and Zaire (Sylvester & Pirmez, 2019)) were plotted to determine whether flow deflection due to Coriolis is likely in these systems. Furthermore, the assessment of whether the observed patterns in submarine channel sinuosity are strongly controlled by latitudinal effects (Peakall et al., 2012) or by other



parameters such as the slope, scale of the channel or flow properties (Peakall et al., 2012; Sylvester & Pirmez, 2019) was carried out.

The digitized channel centerlines and the Python code of Sylvester and Pirmez (2019) that are available on a GitHub repository were downloaded and run to extract channel sinuosities, radii of curvature and latitudes from the nine systems.

It is important to note that the measurement of the radius of curvature in a channel varies among authors and may lead to an inaccurate representation of the scale. The code developed by Sylvester and Pirmez (2019) ensures a robust and homogeneous calculation of radius in all channel bends. The available measurements of radii of curvature then allow for a more reliable comparison against the calculated balance of the Coriolis force and centrifugal force, using  $r$  as a length scale in Equations 1–6 and Equation 8. Also, following Pirmez and Imran (2003), and Sylvester and Pirmez (2019), the radii of curvature are used as a proxy for the scale of the channel. Pirmez and Imran (2003) demonstrated a good correlation between radii of curvature and channel widths in the Amazon Channel. However, we recognize that further work is needed to refine the relationship between channel radii of curvature and width globally with a consistent approach.

### 3. Results

#### 3.1. NAMOC Upper Interface Tilting and Morphometric Relationships

The first ~366 km stretch of the NAMOC is classified as the ‘equilibrium channel’, while the remaining channel length in this data set is classified as the ‘modified equilibrium channel’ due to tributaries joining that affect its morphology (Klaucke et al., 1997; zones 1 and 2, respectively, in Figures 3a and 3b). This part of the work was focused on analyzing changes in the tilt and its relationship with sinuosity and other channel parameters which were not included in the original work of Klaucke et al. (1997). In Figure 3b, each data point corresponds to the tilt estimated at each channel bend.

The NAMOC tilt and sinuosity display high variability throughout the channel length (Figure 3b). The tilt increases downchannel in zone 1 suggesting higher levee asymmetry than zone 2 which displays a decreasing trend. Two peaks above 0.008 m/m correspond to levee collapses in both zones (Klaucke et al., 1997). The sinuosity,  $s_i$ , has a trend that increases from a position at ~120 km (1.01) up to the point of transition between zone 1 and 2 (1.13) with a generally decreasing trend thereafter, albeit with isolated bends displaying sinuosities between 1.10 and 1.15 (Figure 3b). Scatter plots comparing different morphometric parameters against the tilt, sinuosity, and latitude for each channel zone and their calculated  $R^2$  values are shown in Figure 3c.  $R^2$  values are higher in the equilibrium channel section (zone 1) than the modified equilibrium channel where data is very scattered in most cases (zone 2). Plots I, II and III in Figure 3c display weak relationships ( $R^2 < 0.15$ ) in both zones for the downchannel slope against the radius of curvature, sinuosity and tilt, respectively. Plot IV shows the radius of curvature and the tilt have a weak relationship. The tilt against the sinuosity in V has a higher value of  $R^2 = 0.31$  in zone 1, with the sinuosity decreasing as the tilt increases; zone 2 displays a weak relationship with an  $R^2 = 0.02$ . Plots VI, VII and VIII of latitude against sinuosity, downchannel slope and radius of curvature respectively, have weak relationships ( $R^2 < 0.18$ ). The highest  $R^2$  values are observed in zone 1 of Plots IX, X and XI of the latitude against the channel width, tilt and channel height respectively. Latitudes corresponding to zone 1 (between 58° and 60°) show a positive relationship with channel width (plot IX) and height (plot X) with  $R^2$  values of 0.51 and 0.41, respectively. Both width and height decrease with decreasing latitude in zone 1. Channel width in zone 2 (plot IX) shows a negative but weak relationship with latitude; whereas channel height (plot X) also shows a negative but stronger relationship with  $R^2 = 0.32$ , where height increases with decreasing latitude. Latitude-tilt in zone 1 (plot XI) shows the strongest relationship with an  $R^2 = 0.67$  where tilt increases with decreasing latitude, that is, it increases downchannel as seen in Figure 3b; whereas the tilt in zone 2 has a positive but weaker relationship with latitude. Plot XII shows the relationship between channel height and tilt, where the tilt decreases with increasing height in both zones; however, zone 1 exhibits a higher  $R^2$  value of 0.37.

#### 3.2. Comparing Model Predictions of the Tilt to the NAMOC Tilting

The calculated NAMOC tilt  $\gamma_c$  was compared against the measured tilt  $\gamma_m$  with the aim of testing whether the model captured reversal of the upper fluid interface due to strong Coriolis forcing as schematically shown in Figure 2. A positive clockwise  $\gamma_c$  result and a negative anticlockwise  $\gamma_c$  result (Figure 2c) indicates changes in

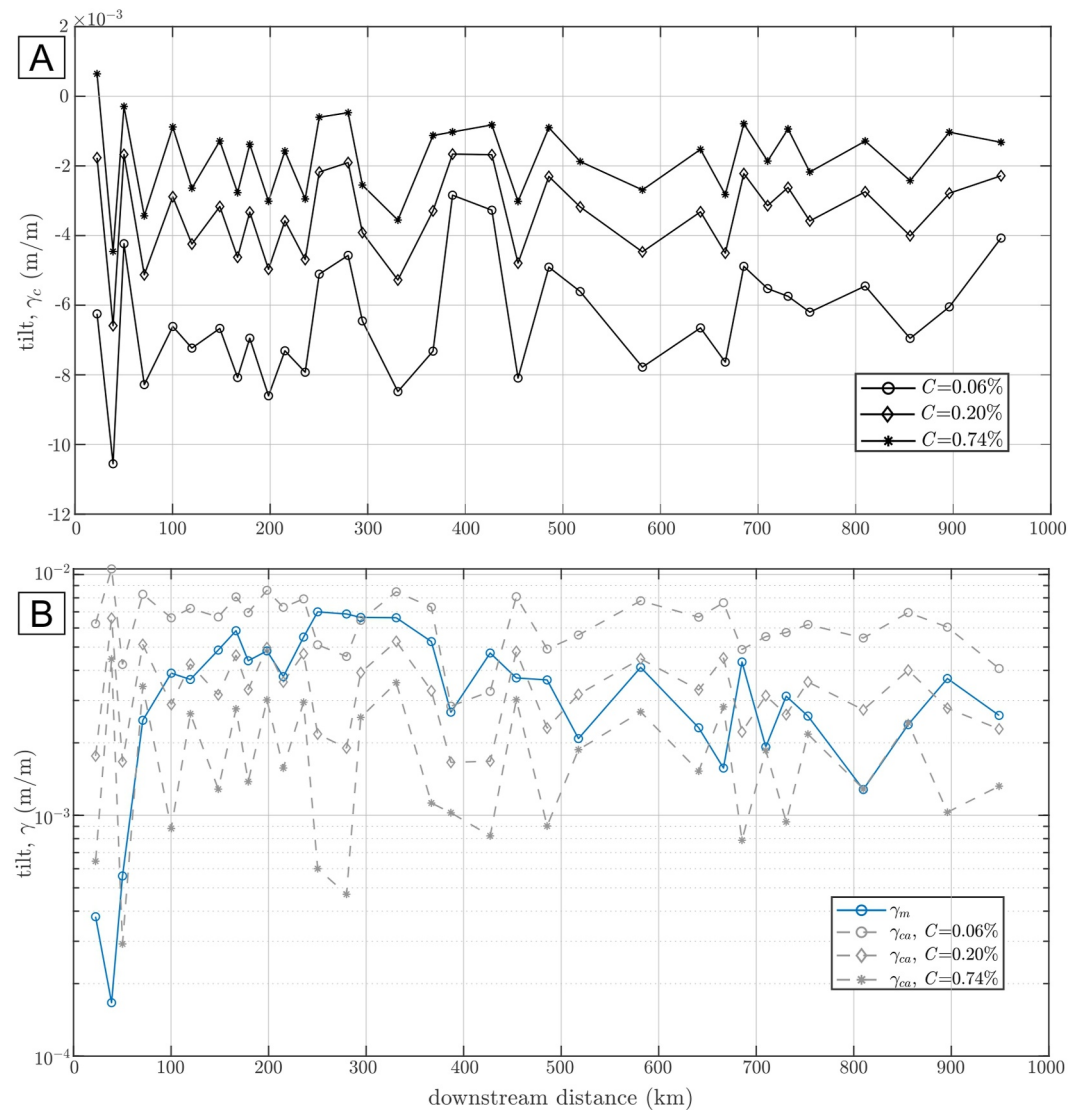


**Figure 4.** Changes in calculated turbidity current tilt for the NAMOC. (a) Calculated tilting from three different sediment concentrations. (b) Absolute values of the calculated tilting compared to the measured tilting.

tilting direction across successive bends. Negative clockwise  $\gamma_c$  results (Figure 2d) indicate that the flow is reversed (i.e., tilting toward the outer bend) such that the tilting would not alternate across bends. Modeling results for the three sediment concentrations in the NAMOC all show negative  $\gamma_c$  values (Figure 4a) (except for one single positive value at the start of  $C = 0.74\%$ ), suggesting that the tilt is reversed for clockwise flows throughout the studied channel stretch (Figure 4a). The calculated reversed tilt supports the suggestion that flow deflection in the NAMOC due to Coriolis forcing produced right-hand side levees that are higher than left levees in both clockwise and anticlockwise flows (Klaucke et al., 1997; Wells & Cossu, 2013).

The absolute slope values of the calculated tilt  $\gamma_{ca}$  compared to the channel tilt  $\gamma_m$  show that  $\gamma_m$  falls within the range of  $\gamma_{ca}$  for the proposed sediment concentrations (0.06%–0.74%) and the tilt values that are closest to  $\gamma_m$  are those associated with a 0.20% sediment concentration, except for the first three channel bends where  $\gamma_m$  is much lower (Figure 4b).  $\gamma_m$  and  $\gamma_{ca}$  range from  $10^{-3}$  to  $10^{-2}$ , although some bends in the calculated flows with  $C = 0.74\%$  derive tilts less than  $10^{-3}$ . Hence,  $\gamma_{ca}$  values suggest that dilute flows have steeper tilts than denser flows (Figure 4b).

These results show that the model makes good predictions of areas of tilt reversal due to Coriolis forcing. This conclusion lends confidence to the results of the following section showing calculations of the variation of tilting

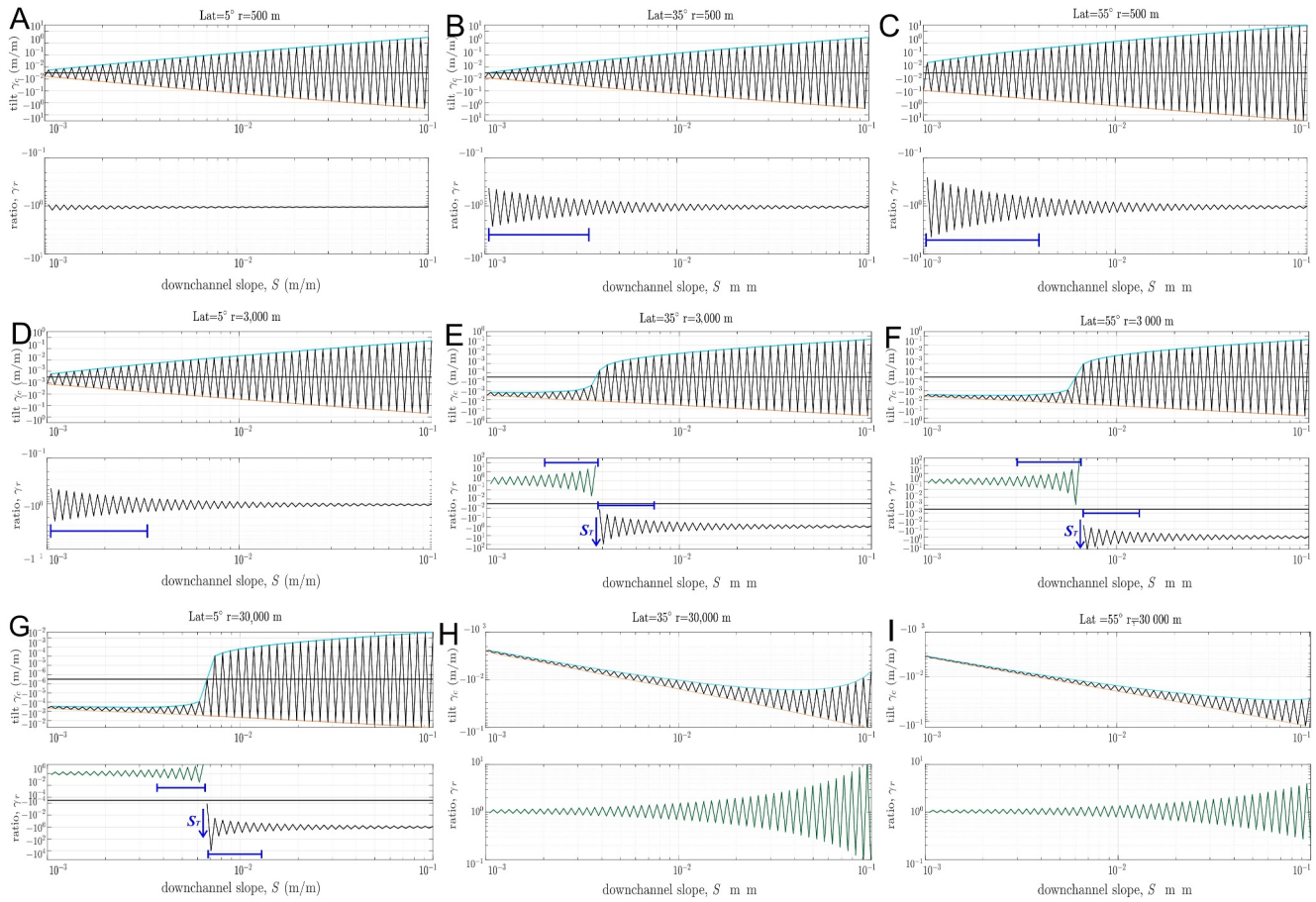


**Figure 5.** Calculated tilting  $\gamma_c$  and ratio  $\gamma_r$  at  $C = 0.02\%$ . The latitude increases in each panel horizontally as  $5^\circ$ ,  $35^\circ$  and  $55^\circ$  (a–c)  $r = 500$  (d–f)  $r = 3$  km (g–i)  $r = 30$  km. Vertical blue arrows indicate the tilting transition slope. Horizontal bars indicate zones of tilting instability.

under different channel and flow conditions; these are used to identify cases where reversal of the upper fluid interface tilt might arise.

### 3.3. Variations in the Tilting of the Upper Fluid Interface

The results of the changes in the upper fluid interface as a function of the radius of curvature, latitude, downchannel slope and sediment concentration are shown in Figures 5 and 6. Furthermore, the analysis of the Rossby number  $Ro_R$  obtained from the scenarios presented in Figures 5 and 6 is shown in Figure 7, where  $Ro_R \gg 1$  describes a centrifugal dominated flow, while  $Ro_R \approx 1$  describes flows where the Coriolis force dominates (Cossu & Wells, 2010; Wells & Dorrell, 2021). Saw-tooth patterns of  $\gamma_c$  follow the sign conventions established in Section 2.3 (Figures 2c and 2d) with peaks corresponding to clockwise bends and troughs to anticlockwise bends. Positive peaks and negative troughs that produce a negative ratio  $\gamma_r$  indicate conditions where the slope of the tilt changes across bends (Figure 2a), whereas negative peaks and troughs that produce a positive  $\gamma_r$  suggest that the tilt in clockwise flows is reversed. Furthermore,  $|\gamma_r| \approx 1$  indicates more stability in the tilting magnitude of  $\gamma_c$  across bends (i.e., that the physical tilting is more similar between consecutive bends) whereas  $1 \ll |\gamma_r| \ll 10$  suggests a less stable tilting.

Dilute flows with  $C = 0.02\%$  traversing bends with small radius of curvatures ( $r = 500$  m) (Figures 5a and 5c) would not experience flow deflection at any latitude, due to the centrifugal force being greater than the Coriolis force as demonstrated by  $Ro_R \gg 1$  in Figure 7a). At low latitudes  $\gamma_r$  is  $\sim 1$  (Figure 5a) and as the latitude increases,  $\gamma_r$  suggests less stability at shallow slopes (Figures 5b and 5c). In the three latitude examples for all radii of curvature,  $\gamma_c$  increases with downchannel slope and flow height (Figures 5 and 6).

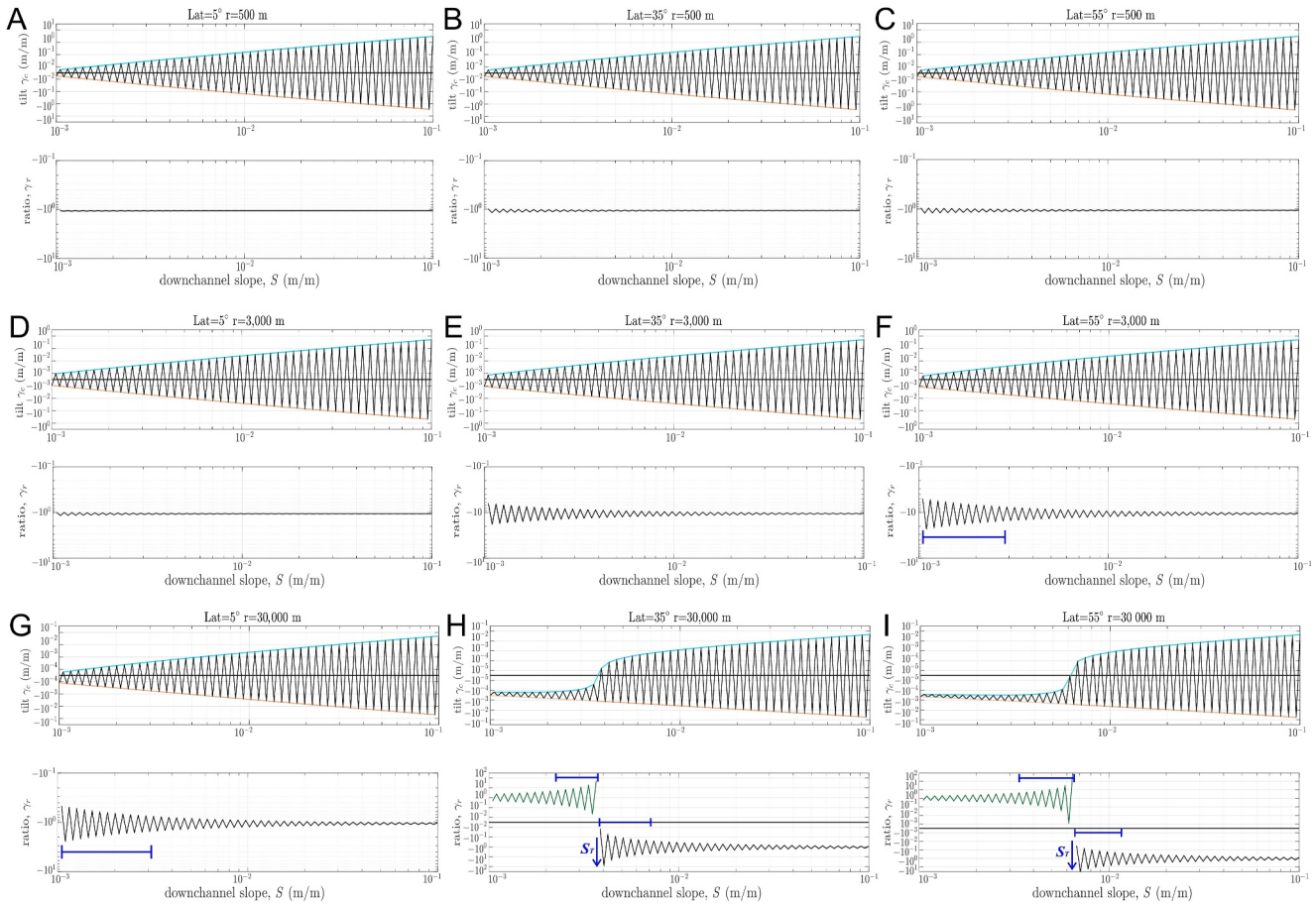


**Figure 6.** Calculated tilting  $\gamma_c$  and ratio  $\gamma_r$  at  $C = 2\%$ . The latitude increases in each panel horizontally as  $5^\circ$ ,  $35^\circ$  and  $55^\circ$  (a–c)  $r = 500$  (d–f)  $r = 3,000$  m (g–i)  $r = 30,000$  m. Vertical blue arrows indicate the tilting transition slope. Horizontal bars indicate zones of tilting instability.

Flows traversing bends with intermediate radii of curvature ( $r = 3,000$  m) at low latitudes (Figure 5d) would not experience flow deflection ( $|R_{O_R}| \gg 1$ , Figure 7b); however, the stability of the tilt decreases at shallow slopes. As the latitude increases to  $35^\circ$  (Figures 5e) and  $55^\circ$  (Figure 5f), the saw-tooth shape pattern becomes negative and the ratio becomes positive at shallow slopes, suggesting that flow deflection occurs at a given downchannel slope, that is, close to the tilt transition slope  $S_T$  (Figure 2e), where  $|R_{O_R}| \approx 1$  (Figure 7b). The point of transition moves toward steeper slopes as the latitude increases (Figure 5f). Furthermore, the ratio shows that the stability of the tilt decreases near the transition point and stabilizes away from it (Figures 5e and 5f).

At larger radii of curvature ( $r = 30,000$  m), flow deflection is observed at  $5^\circ$  (Figures 5g)  $35^\circ$  (Figures 5h) and  $55^\circ$  (Figure 5i) of latitude. The transition slope also moves toward steeper slopes from low to high latitudes. At  $35^\circ$  and  $55^\circ$  latitudes, positive  $\gamma_r$  values cover the entire downchannel slope range and  $|R_{O_R}| \approx 1$  (Figure 7c).

The tilts of denser flows with  $2\%$  (Figure 6) shows similar trends to those of dilute flows, where  $\gamma_c$  increases with downchannel slope and flow height. Also, at small radii of curvature (Figures 6a–6c) and at intermediate values ( $r = 3,000$  m) at  $5^\circ$  latitude (Figure 6d) flow deflection is not observed ( $|R_{O_R}| \gg 1$ , Figures 7a and 7b). Differences between dilute and denser flows are seen in areas of flow deflection. The tilt of flows with  $C = 2\%$  do not suggest flow deflection at any of the modeled latitudes when  $r = 500$  m (Figures 6a–6c) and  $3,000$  m (Figures 6d–6f), nor at  $5^\circ$  latitude when  $r = 30,000$  m (Figure 6g). Flow deflection is only predicted at  $35^\circ$  and  $55^\circ$  latitudes for large radius (Figures 6h and 6i) and occurs at  $|R_{O_R}| < 1.05$  (Figure 7c). Furthermore,  $|R_{O_R}|$  for a given radius and latitude increases with  $C$  (Figure 7). Values of  $\gamma_r$  in denser flows are closer to 1, suggesting higher stability than in dilute flows. Also, comparing the same flow, latitudinal and slope conditions for three different radius of curvature (Figures 5c–5i and Figures 6c, 6f, 6i) it is also noted that the latter has a stronger impact in the balance of Coriolis and centrifugal forces. The location of the transition point has a stronger shift in its slope position



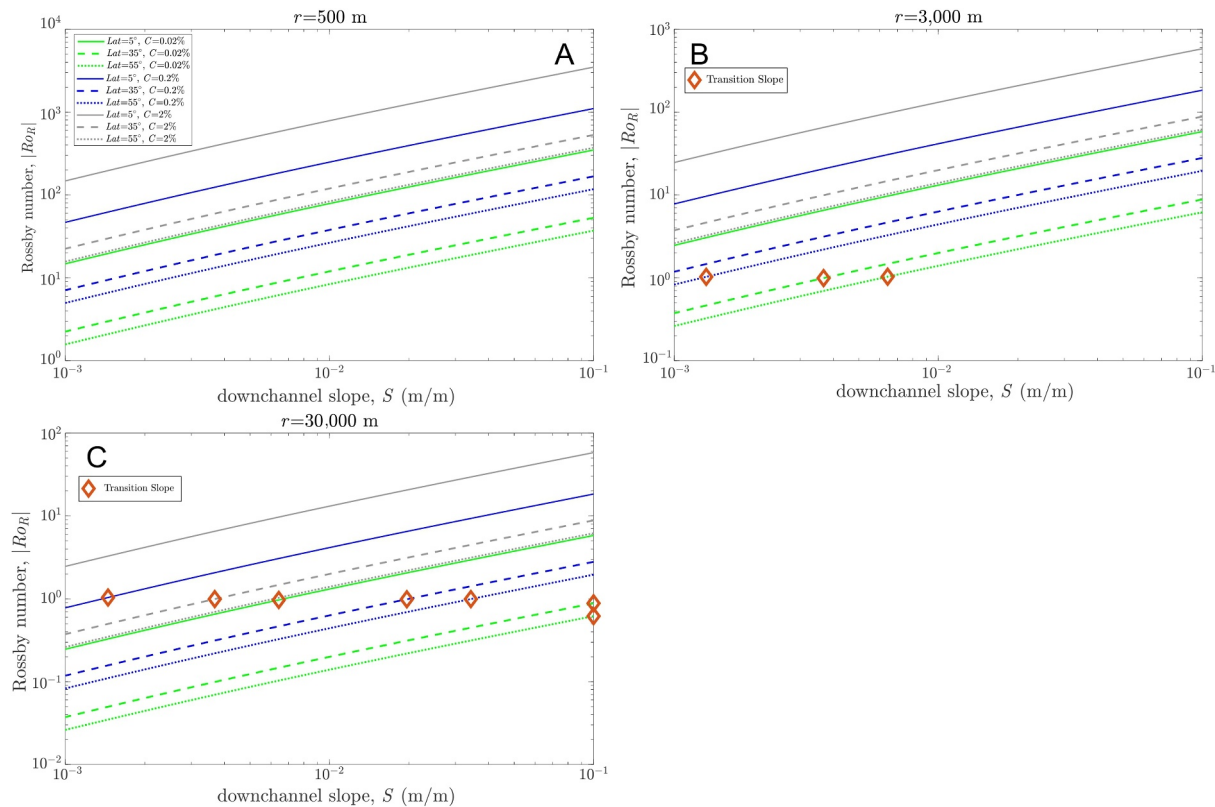


**Figure 7.** Calculated absolute Rossby number as a function latitude, sediment concentration and radius of curvature for (a) small,  $r = 500$  m (b) intermediate,  $r = 3,000$  m and (c) large,  $r = 30,000$  m, bends. The diamonds represent the transition slopes. At the transition slope, the Rossby number is  $\sim 1$ , therefore, Coriolis force dominates and the upper interface tilt is reversed.

compared to flows under the same conditions for different latitudes. These might suggest a higher sensitivity of the set of equations used to  $r$  compared to the other parameters, together with the sediment concentration.

### 3.4. Variations in the Tilting Transition Slope $S_T$

The identification of flow deflection occurring at a specific downchannel transition slope,  $S_T$  motivated further investigation of where the transition might occur under a broader set of channel and flow conditions. Thereby,  $S_T$  values that would promote flow deflection were determined as a function of the scale of the bend, latitude and flow conditions.

$S_T$  is proportional to the radius of curvature but inversely proportional to sediment concentration (Figure 8a). The transition slope increases with radius of curvature from  $\sim 10^{-7}$  at  $r = 300$  m to  $\sim 10^{-2}$  at  $r = 60,000$  for  $C = 1\%$ , therefore, small bends have lower transition slopes than large bends. As the flow density decreases,  $S_T$  increases up to  $\sim 10^{-5}$  to  $> 10^{-0}$  at small and large bends respectively. Dense flows ( $\geq 1\%$  bulk sediment concentration) have lower transition slopes than dilute ( $\ll 1\%$  bulk sediment concentration) flows for a given radius of curvature. Similarly,  $S_T$  increases with a decreasing flow height, where deep flows have lower transition slopes than shallow flows (Figure 8b). The variation of  $S_T$  with latitude shows that transition slopes are proportional to latitude (Figure 8c). For a given radius  $S_T$  increases as the latitude increases. Channels at low latitudes and small radius of curvature have the lowest transition slopes; whereas, large radius channels at high latitudes have the steepest. Furthermore, little change is observed in  $S_T$  contours at latitudes above  $60^\circ$ .

### 3.5. Tilting Transition Slopes and Global Submarine Channel Data

The latitude, sinuosity and radii of curvature from nine submarine channels were obtained from Sylvester and Pirmez (2019): Amazon (Pirmez & Flood, 1995), Danube (Popescu et al., 2004), Knight Inlet (Ren et al., 1996), Monterey (Fildani & Normark, 2004), NAMOC (Klaucke et al., 1997), Nile (Migeon et al., 2010), Rhone (Torres



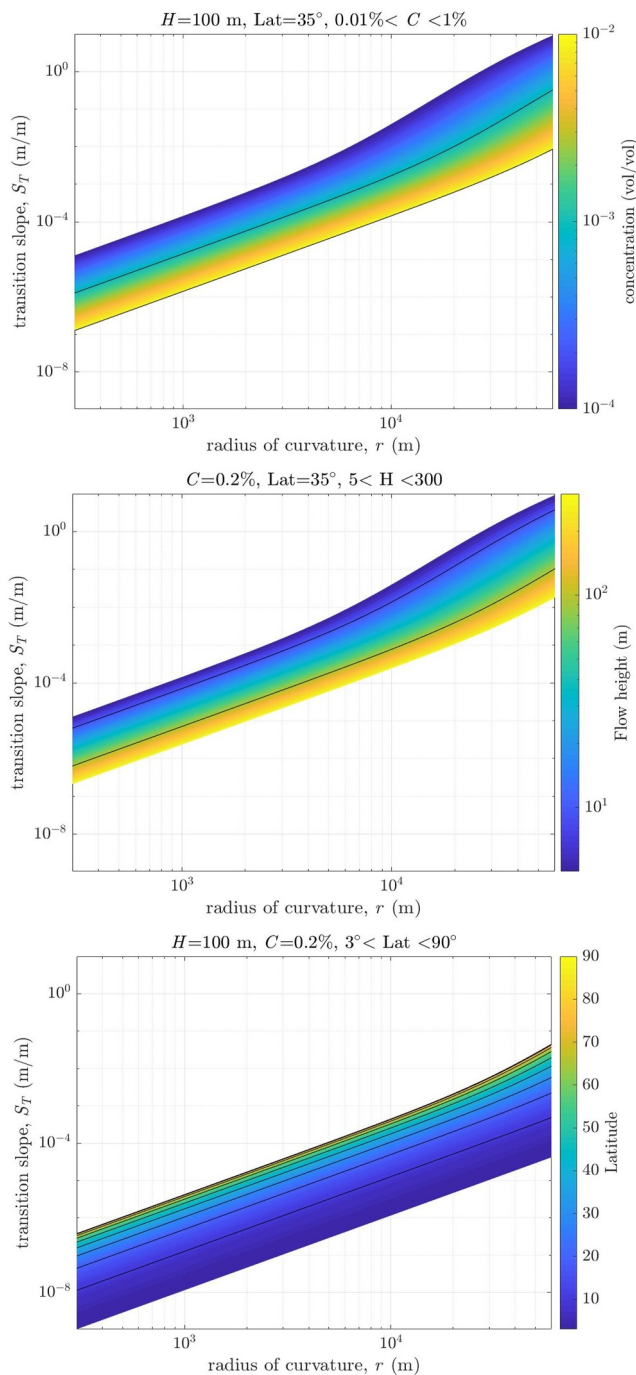


**Figure 8.** Changes in the calculated tilting transition slope with (a) sediment concentration (b) flow height and (c) latitude. If the downstream slope of a channel at a specific radius and latitude is less than the transitional slope, then it is likely to be strongly influenced by the Coriolis force.

velocities of 2 m/s, the radius of curvatures in channels must be in the order of  $\sim 10$  km or greater for Coriolis forcing to exceed the centrifugal force in the lower, confined portion of the flow that shapes the channel. Additionally, Sylvester and Pirmez (2019) suggested that as flow velocities decrease, the balance of forces tends to shift in favor of the Coriolis effect, even in smaller systems. Consequently, they proposed that the dilute and slow upper layers of the current are more susceptible to the influence of the Coriolis effect, even at low latitudes; whereas the lower fast-moving portion of the flow is dominated by the centrifugal force. The latter phenomenon is

et al., 1997), Tanzania (Bourget et al., 2008) and Zaire (Babonneau et al., 2002) (Figure 9). These channel systems span latitudes from  $3^\circ$  (Amazon) to  $60^\circ$  (NAMOC) and show the sinuosity for every channel bend (Figure 9a). The lowest maximum sinuosities are observed in the Tanzania channel and NAMOC, with peak sinuosities of 1.11 and 1.15, respectively (Figure 9a). The Rhone and Monterey channels follow with 1.62 and 2.35, respectively. The Danube, Zaire and Amazon channels have a peak sinuosities of 3.46, 3.5 and 4.1, respectively. Although most bends in the Knight Inlet have sinuosity values of less than 2.7, its peak sinuosity is 4.24; similarly, although most bends in the Nile channel are under 3.2, its highest sinuosity is 4.7. The data spans radii of curvature of several orders of magnitude (from  $\sim 91$  up to  $\sim 14,800$  m) and show that sinuosity decreases with increasing radius of curvature (Figure 9b).

Contour plots of calculated  $S_T$  versus, latitude plus the Sylvester and Pirmez (2019) channel data are shown in Figure 10. Data symbols correspond to the mean radius of curvature and vertical bars extend to the minimum and maximum radius of curvature measured at each channel bend (Figure 9b). Colored  $S_T$  contours match channel symbols according to the magnitude of their downchannel slope.

The values of the  $S_T$  contours increase as radius of curvature and latitude increase for all the flow conditions modeled (Figures 10a–10d). For the case of a deep and dilute current, most channels plot below their corresponding contour (Figure 10a). The mean radius of Tanzania is proximal to its contour ( $10^{-3}$ ) whereas the NAMOC mean radius is located above it ( $10^{-4}$ ) by one order of magnitude (Figure 10a). As the sediment concentration increases, the contours decrease for a given latitude and radius (Figure 10b). Therefore, channels plot further below their corresponding contour.  $S_T$  contours of a shallow and dense turbidity current show a similar relationship as those for deep and dilute (Figure 10c), where channels plot below their contours except for the NAMOC. As sediment concentration decreases, the contours increase for a given latitude and radius, and many channels plot close to or above their corresponding contour (Figure 10d).

#### 4. Discussion

Peakall et al. (2012), Cossu and Wells (2013), and Wells and Cossu (2013) hypothesized that Coriolis forcing - induced reversals to the tilt of the upper interface of channelized turbidity currents promotes the development of low sinuosity channels at high latitudes, whereas, the predominance of centrifugal forcing near the Equator promotes sinuous channel development. Furthermore, Peakall et al. (2012) proposed a  $50^\circ$  latitude cut-off for the development of high-sinuosity channels based on the analysis of peak channel sinuosities and their latitudinal position. However, Sylvester and Pirmez (2019) challenged the concept of latitudinal control due to Coriolis and proposed that the Coriolis force is weak and is unlikely to be responsible for the low sinuosity channels observed in some systems. Instead, they argued that the size of the channel and flow velocity have a more important role in determining the impact of Coriolis. Sylvester and Pirmez (2019) suggested that at current

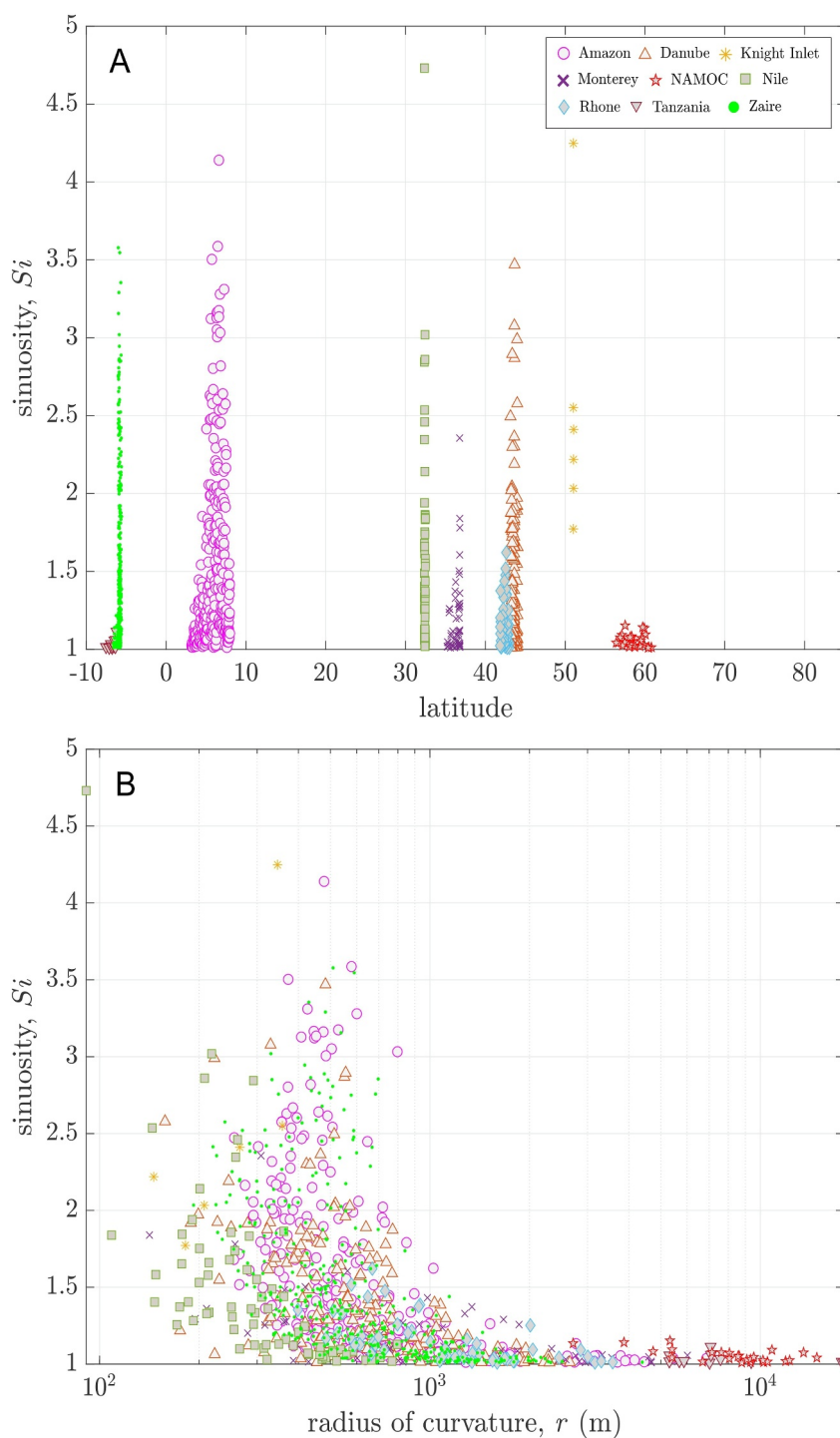


**Figure 9.** Global channel data extracted from Sylvester and Pirmez (2019). (a) Latitude versus sinuosity and (b) radius of curvature versus sinuosity.

exemplified by the Danube channel system (discussed in the following sections), which is high-latitude with a strong levee asymmetry yet displays a highly sinuous planform.

The following sections discuss the observed controls on the changes in the tilting and  $S_T$  within the context of the debate on whether a strong latitudinal control exists for the development of channel sinuosity.

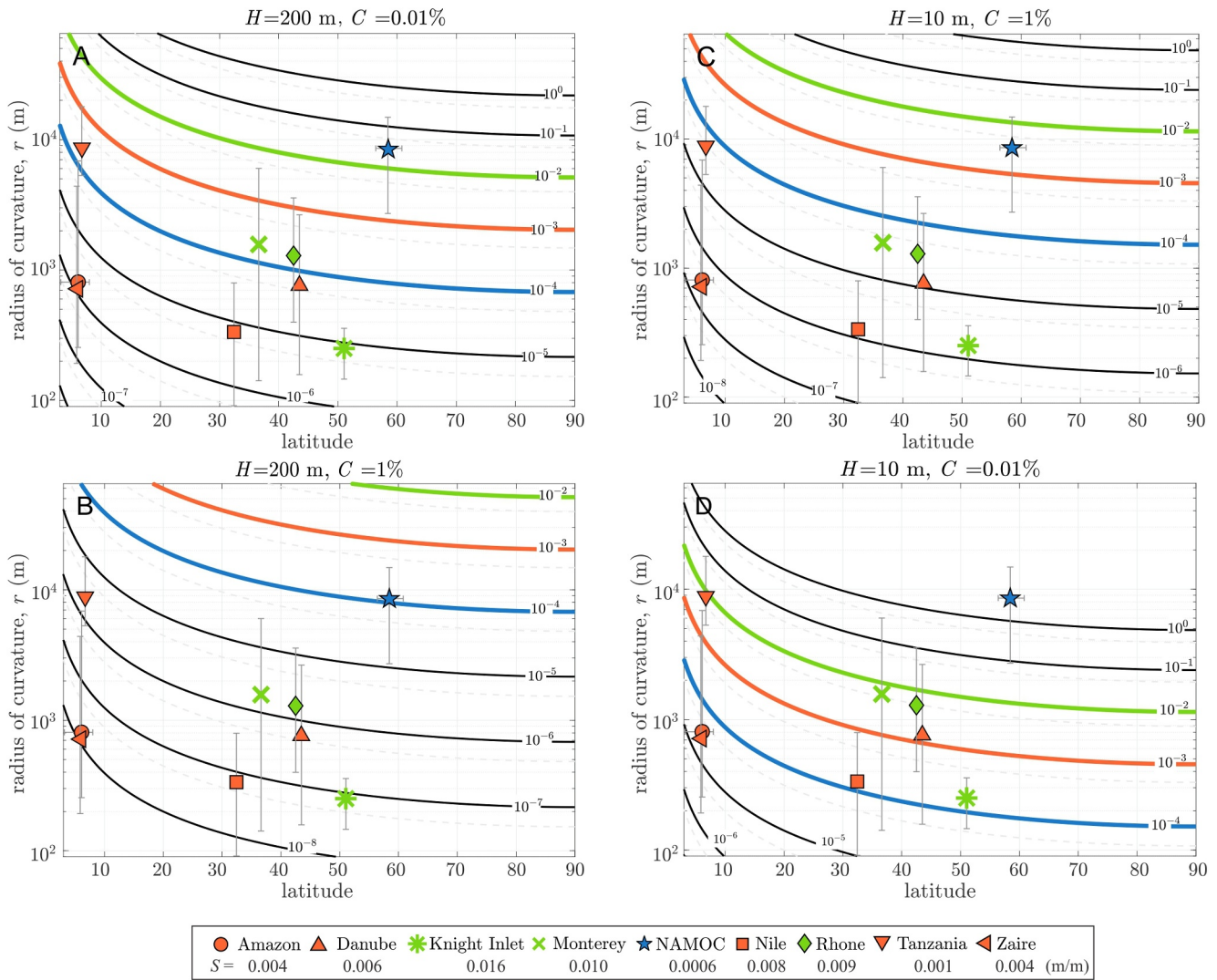


**Figure 10.** Contours of the tilting transition slope co-plotted with seafloor channel data from Sylvester and Pirmez (2019) as a function of latitude and radius of curvature for (a) deep and dilute currents, (b) deep and dense currents, (c) shallow and dense currents and (d) shallow and dilute currents. The colors of each symbol match the contour with the magnitude of the downchannel slope in each system. When the contour is above its corresponding symbol ( $S > S_T$ ), the channel is likely to develop sinuous bends. When it is below the symbol ( $S < S_T$ ), the channel is likely to straighten.

#### 4.1. Controls on the Effect of Coriolis Based on Changes in the Upper Fluid Interface Tilting

The results from the changes in tilting suggest that both the latitudinal position and scale of the channel (here analyzed through the radius of curvature) control the impact of Coriolis (as previously suggested by Imran et al. (1999)), providing that other conditions are met in terms of the downchannel slope and flow conditions (Figures 5–8).

Figures 5 and 6 also show that the effect of the Coriolis force is diminished in large scale channels as latitude decreases; Imran et al. (1999) also showed this trend in the NAMOC where the Coriolis force had a weak influence on the channel for a latitude of 6° despite its large scale.

Dilute turbidity currents ( $\ll 1\%$  bulk sediment concentration) traveling over shallow slopes in large scale systems ( $r = 30,000$ ) represent conditions where the Coriolis force more likely exceeds the centrifugal force (Figure 5), therefore promoting flow deflection that could limit bend expansion and sinuosity development, even at latitudes as low as 5° (Figure 5g); this value differs significantly from the 50° cut-off value proposed by Peakall et al. (2012). Dilute flows on shallow slopes would also experience flow deflection in mid-scale channels with

$r = 3,000$  at  $35^\circ$  and  $55^\circ$  latitudes, which shows that the effect of Coriolis can be significant at radius of curvature much lower values than the  $\sim 10$  km value proposed by Sylvester and Pirmez (2019).

The modeled conditions at  $55^\circ$  show that in small scale channels ( $r = 500$ ), the Coriolis force cannot exceed the centrifugal force at any given downchannel slope. Hence, tilt reversal would not occur and sinuous channels may form. However, some of the examples that do not show a reversed tilt do suggest that the stability of the tilt is poor (Figure 5c). The lack of tilting stability translates into anticlockwise tilts being superelevated and clockwise tilts  $\approx 0$  due to the increase in Coriolis forcing (Wells & Dorrell, 2021). Therefore, Coriolis forces may shift the location of the velocity and density core before the upper interface is reversed, as experimental observations have shown (Davaranah Jazi et al., 2020). A measure of the early deflection may be approximated through the observation of tilt instabilities. Thus, areas of poor tilting stability found in both dilute and dense currents over shallow slopes at  $35^\circ$  and  $55^\circ$  latitudes might experience flow deflection. Furthermore, the observed tilting instability near  $S_T$  suggest that flow deflection might occur earlier than the results predict (Figures 5 and 6). At low latitudes, potential instability zones are limited to mid-radius in dilute flows (Figure 5d) and large radius in dense flows (Figure 6g). Changes in  $\gamma$ , also suggest that dense currents (Figure 6) can maintain a more stable normal tilting across bends (i.e., the effect of Coriolis is hampered) compared to dilute flows which are more susceptible to the Coriolis effect. The latter would then support the suggested behavior by Sylvester and Pirmez (2019) stating that the lower denser portion of the current is more centrifugal dominated, while the upper more dilute portion is more influenced by Coriolis. However, the results would also suggest that the force balance in a more dilute lower portion of the current could be Coriolis-dominated (as well as in the upper portion of the flow as suggested by Sylvester and Pirmez (2019)) even at bends with radius less than  $\sim 10$  km (Figures 5e and 5f).

#### 4.2. Controls on the Tilting Transition Slope and Implications for the Development of Sinuosity in Submarine Channels

The tilting transition slope  $S_T$  defines the minimum (threshold) downchannel slope needed in a system for sinuosity development and the analysis shows that it is dependent on flow conditions as well as the channel radius and latitude (Figure 8), rather than being solely controlled by latitude. If downchannel slopes in the system are steeper than their calculated threshold for a given latitude, radius and flow conditions (i.e., when contours are above their corresponding colored symbol in Figure 10), then sinuosity development would be promoted. In contrast, if the downchannel slope is lower than the threshold (i.e., contours are below their corresponding colored symbols in Figure 10), sinuosity would be hindered by the effect of Coriolis forcing. Therefore, the lower  $S_T$  values observed in low latitudes, small bends, dense ( $\geq 1\%$  bulk sediment concentration) and deep flows (Figure 8) equate to a lower threshold which would facilitate the development of sinuosity under these conditions. On the other hand, higher  $S_T$  values in large bends, dilute ( $\ll 1\%$  bulk sediment concentration) and shallow flows at high latitudes (Figure 8) are equivalent to higher thresholds that would make the development of sinuosity more difficult.

The changes on threshold conditions and the associated implications for the development of sinuosity may therefore provide an explanation for the observations of Sylvester and Pirmez (2019) that the Nile, Danube and Knight Inlet channels have high sinuosity bends despite being located at high latitudes and that the low latitude Tanzania channel has a low sinuosity. Although the Nile and Knight Inlet are small scale channels (bends  $< 10^{-3}$ ) with their threshold  $S_T$  between  $10^{-7}$  to  $10^{-4}$  for different flow conditions, the magnitude of the downchannel slopes in both systems (orange and green contours, respectively) are steep enough to exceed threshold conditions in all cases (Figures 10a–10d) (i.e., contours are always above their corresponding symbols), hence suggesting that the Coriolis force would not exceed the centrifugal force, therefore allowing for sinuosity development. The Nile and Knight Inlet (located above the  $50^\circ$  cut-off) have peak sinuosities  $> 4$  (Figure 9). Therefore, in these cases the scale of the channels and slopes are stronger controls than the high latitudinal position. Similarly, centrifugal forces are stronger than Coriolis forces in the Danube and Rhone channels as the threshold slope is exceeded by the downchannel slopes (orange and green contours, respectively) under most flow conditions (Figures 10a–10c). Nevertheless, shallow and dilute flows traversing the larger channel bends in these systems (i.e.,  $> 10^{-3}$ ) represent a scenario where flow deflection might occur due to Coriolis and therefore bend growth would be stopped or reduced (Figure 10d).

The downchannel slopes for other sinuous channels like the Amazon, Zaire (orange contours) and Monterey (green contours) show that they exceed threshold conditions for most flows (contours above their corresponding



symbols), which suggests that sinuous bends would be promoted even if these channels were located at higher latitudes (Figures 10a–10c). In the case of the Amazon channel, it was also demonstrated by Imran et al. (1999) that the effect of the Coriolis force is weak in the channel at low and high latitudes for its scale.

Similarly to other channels, only shallow-dilute flows ( $\ll 1\%$  bulk sediment concentration) could experience flow deflection in Zaire and Monterey. However, this scenario might not happen in these channels as natural flow data from these settings have registered thicker flows with higher sediment concentration (Vangriesheim et al., 2009; Xu et al., 2014).

The low sinuosity, low latitude Tanzania channel has a slope that is equivalent in magnitude to its low latitude but sinuous Amazon and Zaire equivalents. However, the Tanzania channel has bends that are an order of magnitude larger; therefore, its threshold  $S_T$  is higher, which makes the channel more prone to flow deflection than the Amazon and Zaire. The flow conditions that may suggest flow deflection in the channel, hence promoting low sinuosity, are deep and dilute (Figure 10a) and shallow - dilute flows (Figure 10d). Deep and dilute flows in the Tanzania channel approximate threshold conditions, therefore, tilt instability and flow deflection due to Coriolis may arise. On the other hand, shallow-dilute flows suggest flow deflection throughout the channel as channel slopes (orange contour) are lower (below) than the channel threshold  $S_T$ . The Tanzania channel has a peak sinuosity of 1.1.

The NAMOC is the only channel in this data set consistently showing that the downchannel slopes do not exceed its calculated threshold  $S_T$ . The Coriolis force would exceed the centrifugal force throughout the channel length not only for its high latitudinal position but also for its large-scale bends and shallow slopes compared to other systems. This combination of factors potentially controlling sinuosity in the NAMOC might explain why individual morphometric relationships of channel sinuosity are weak (Figure 3) and why the NAMOC has very low sinuosity.

The NAMOC and the Danube channels display a strong levee asymmetry, which previous studies have attributed to the Coriolis effect (Klaucke et al., 1997; Popescu et al., 2001). However, a critical difference between these two systems, as demonstrated by our findings, is that centrifugal forces exert a stronger influence than Coriolis forces in the Danube channel (Figure 10). Consequently, this force balance fails to account for the significantly higher right levee in the channel. An alternative explanation follows the idea by Sylvester and Pirmez (2019) suggesting that the lower, denser portion of the flow is dominated by centrifugal forces, while the more dilute upper portion is dominated by Coriolis forces. This decoupling of the forces would cause the upper flow to deflect and ultimately result in the formation of higher right-hand side levees.

The calculation of  $S_T$  shows that the observed changes in channel sinuosity are not solely nor strongly controlled by latitude, but by a combination of factors such as flow density, flow depth, downchannel slope and channel size would either promote or hinder bend growth; which is in line with the suggestion of Sylvester et al. (2013) and Sylvester and Pirmez (2019) that slope and flow type must also have a major control on channel sinuosity. Hence, the results shown provide an explanation for high sinuosity channels being developed at high latitudes or low sinuosity channels near the equator. Systems such as the Tanzania and NAMOC demonstrate to be influenced by Coriolis (although the Tanzania only by specific flow conditions, see discussion above), despite the significantly different latitudinal position (Figure 10). It is also demonstrated that typical turbidity currents in most channel systems are more likely to exceed threshold conditions (Figure 10); hence, the force balance at channel bends would be centrifugal-dominated and their sinuosity development would not be hindered by Coriolis forces; this outcome is also supported by the work of Sylvester and Pirmez (2019).

Given that the latitude, radius and downchannel slope are parameters that can be easily approximated in a system, the calculated  $S_T$  contours may be used to screen the likelihood of developing sinuous channels in other turbidite systems. If the downstream slope of a channel at a specific radius and latitude is less than the threshold slope  $S_T$ , then the channel is likely to be strongly influenced by the Coriolis force and hinder sinuosity development.

### 4.3. Limitations and General Recommendations

Although the application of this turbidity current modeling technique may permit a better understanding of the dynamics of critical processes in deepwater environments, it is important to recognize the present limitations of the approach.



The upper interface tilt is used as a proxy to determine whether a submarine channel is likely to develop a sinuous planform or not. The experimental work of Wells and Cossu (2013) in straight and sinuous channels demonstrates the influence of the Coriolis force on the upper interface tilt, the velocity maximum and their link to erosional and depositional patterns that lead to low or high sinuosity channels; which later was reinforced by Davarpanah Jazi et al. (2020). Hence, our assumption of linking the changes in the tilt to the likelihood that a channel has to be sinuous or straight stands valid. However, it is recognized that here the cross-sectional levee asymmetry of the NAMOC is assumed to represent the turbidity current upper fluid interface tilt; nevertheless, measurements of the cross-sectional flow properties in natural channels have shown that the flow tilting may not be equal to the cross-channel asymmetry (Parsons et al., 2010; Sumner et al., 2014), particularly for superelevated flows at channel bend apices (Straub et al., 2008). Therefore, the upper interface tilting in real flows may be higher (or possibly lower in other cases) than the gradient suggested by the channel geometry.

Given the lack of solid knowledge on the variations of the interface tilting in natural flows, the approximations through the channel-levee asymmetry might constitute the best guess. Further investigations on the variations and controls of the interface tilting would be needed to better constrain this parameter, ideally through the observations of cross-sectional channel profiles of density and velocity from natural currents.

The assumed depth-averaged velocity and density of the current do not allow for the incorporation of the effect of vertical velocity variation and stratification (Dorrell et al., 2014; Sumner & Paull, 2014). Davarpanah Jazi et al. (2020) demonstrated that, under specific experimental conditions where Coriolis forces are stronger than centrifugal forces, decoupling of the density and velocity fields exists, with the density maximum being influenced by the centrifugal force and the velocity maximum by the Coriolis force (see Introduction for further details), which is not possible to capture by the model used in this work. However, we can speculate that in the limited conditions examined here where the Coriolis force dominates (e.g., the NAMOC), the velocity maximum is shifted as is the upper interface tilting (or where the tilting is flat (Figure 2e) as schematically shown by Davarpanah Jazi et al. (2020)), causing greater erosion in the right-hand side banks for the Northern Hemisphere (left-hand side for the Southern Hemisphere), high levee asymmetry and limiting bend growth.

## 5. Conclusions

Reversal of the tilt of the upper fluid interface of turbidity currents between successive channel bends has been associated with the development of channel sinuosity, whereas tilt orientations that do not reverse have been associated with the development of low-sinuosity channels. Here, we present a new method for calculating the tilt of bend-traversing turbidity currents under different combinations of latitude, channel size, channel axis slope, flow size and flow density, to show that.

1. Approaches to understanding channel sinuosity development based solely on slope or latitude, where channels on higher slopes are less sinuous than those on lower slopes (Clarke et al., 1992) or where high latitude channels are less sinuous than equatorial channels (Peakall et al., 2012) do not capture the full spectrum of possible controls on channel sinuosity. Thus, a combination of factors including variations in downchannel slope, channel size, flow conditions and to a lower degree, latitudinal position, are more likely to determine the tendency of channels to become sinuous.
2. Parametric analysis shows that the development of sinuous channels is strongly promoted by the passage of deep and dense ( $\geq 1\%$  bulk sediment concentration) flows through small or mid-size channels (with bends in the order of tens to thousands of meters) located in mid to steep slope gradient systems (i.e., above the order of  $10^{-3}$ ) at all latitudes; that is, the current exhibits a normal upper interface slope throughout the channel bends and sinuosity suppression due to Coriolis is not significant (e.g., the Knight Inlet, Amazon and Nile channels). Whereas a limited case of dilute ( $\ll 1\%$  bulk sediment concentration) and shallow flows in large-scale channels (with bends close or in the order of tens of kilometers) have a reduced possibility of developing sinuous channel planforms at all latitudes; that is, the current experiences a reversal in the upper interface tilt and a shift of the locus of erosion and deposition due to Coriolis (e.g., the NAMOC and Tanzania channel). However, based on the data set assessed here from Sylvester and Pirmez (2019), this large bend scale is rare in real-world channels.
3. The calculation of a channel slope threshold across which tilting behavior changes can help to better understand the observed sinuosity variations in nine analyzed modern channels. It is demonstrated that typical turbidity currents in most channel systems are more likely to exceed threshold conditions. Consequently, at

channel bends, the dominant force balance leans toward centrifugal forces, and the development of sinuosity is not hampered by Coriolis forces. Further work, either through experimental or numerical approaches, should consider the multifactorial effect and further investigate the effect of the concentration on the development of submarine channel sinuosity.

- The channel slope thresholds may be applicable to other channels systems to determine whether for the given slope gradient, channel size, latitude and flow conditions (if known) the channel is likely to meander or straighten. It follows that if the channel evolution style can be constrained for such channels, then flow conditions might be estimated.

## Data Availability Statement

The data and the MATLAB script that forms the basis of the code used in this research is available online through White Rose eThesis Online under Appendices C and D (Crisóstomo-Figueroa, 2022) (<https://etheses.whiterose.ac.uk/31764/>).

## Acknowledgments

We thank CONACYT-SENER and the Turbidites Research Group sponsors (AkerBP, CNOOC, ConocoPhillips, Harbour, Murphy, OMV, Oxy and PetroChina) for funding the research project under which this work was undertaken. Dr Ingo Klaucke is thanked for providing morphometric data and maps for the analysis of the NAMOC. Two anonymous reviewers are thanked for their thorough reviews that greatly improved the manuscript.

## References

- Abad, J. D., Sequeiros, O. E., Spinewine, B., Pirmez, C., Garcia, M. H., & Parker, G. (2011). Secondary current of saline underflow in a highly meandering channel: Experiments and theory. *Journal of Sedimentary Research*, 81(11), 787–813. <https://doi.org/10.2110/jsr.2011.61>
- Abreu, V., Sullivan, M., Pirmez, C., & Mohrig, D. (2003). Lateral accretion packages (LAPs): An important reservoir element in deep water sinuous channels. *Marine and Petroleum Geology*, 20(6–8), 631–648. <https://doi.org/10.1016/j.marpetgeo.2003.08.003>
- Babonneau, N., Savoye, B., Cremer, M., & Klein, B. (2002). Morphology and architecture of the present canyon and channel system of the Zaire deep-sea fan. *Marine and Petroleum Geology*, 19(4), 445–467. [https://doi.org/10.1016/S0264-8172\(02\)00009-0](https://doi.org/10.1016/S0264-8172(02)00009-0)
- Bourget, J., Zaragosi, S., Garland, T., Gabelotaud, I., Guyomard, P., Dennielou, B., et al. (2008). Discovery of a giant deep-sea valley in the Indian Ocean, off eastern Africa: The Tanzania channel. *Marine Geology*, 255(3–4), 179–185. <https://doi.org/10.1016/j.margeo.2008.09.002>
- Clare, M., Lintern, D. G., Rosenberger, K., Clarke, J. E. H., Paull, C., Gwiazda, R., et al. (2020). Lessons learned from the monitoring of turbidity currents and guidance for future platform designs. *Geological Society - Special Publications*, 500(1), 605–634. <https://doi.org/10.1144/SP500-2019-173>
- Clark, J. D., Kenyon, N. H., & Pickering, K. T. (1992). Quantitative analysis of the geometry of submarine channels: Implications for the classification of submarine fans. *Geology*, 20(7), 633–636. [https://doi.org/10.1130/0091-7613\(1992\)020<0633:qaotgo>2.3.co;2](https://doi.org/10.1130/0091-7613(1992)020<0633:qaotgo>2.3.co;2)
- Coleman, T. F., & Li, Y. (1996). An interior, trust Region approach for nonlinear minimization subject to bounds. *Society for Industrial and Applied Mathematics Journal on Optimization*, 6(2), 418–445. <https://doi.org/10.1137/0806023>
- Cossu, R., & Wells, M. G. (2013). The evolution of submarine channels under the influence of Coriolis forces: Experimental observations of flow structures. *Terra Nova*, 25(1), 65–71. <https://doi.org/10.1111/ter.12006>
- Cossu, R., Wells, M. G., & Peakall, J. (2015). Latitudinal variations in submarine channel sedimentation patterns: The role of coriolis forces. *Journal of the Geological Society*, 172(2), 161–174. <https://doi.org/10.1144/jgs2014-043>
- Cossu, R., Wells, M. G., & Whlin, A. K. (2010). Influence of the Coriolis force on the velocity structure of gravity currents in straight submarine channel systems. *Journal of Geophysical Research*, 115(C11), 1–15. <https://doi.org/10.1029/2010JC006208>
- Cossu, R., & W, M. G. (2010). Coriolis forces influence the secondary circulation of gravity currents flowing in large-scale sinuous submarine channel systems. *Geophysical Research Letters*, 37(17), 1–6. <https://doi.org/10.1029/2010GL044296>
- Crisóstomo-Figueroa, A. (2022). *Calculating hydraulic conditions of turbidity currents from surficial and subsurface deepwater channel architecture*. Unpublished thesis of the University of Leeds.
- Davarpanah Jazi, S., Wells, M. G., Peakall, J., Dorrell, R. M., Thomas, R. E., Keevil, G. M., et al. (2020). Influence of Coriolis force upon bottom boundary layers in a large - scale gravity current experiment: Implications for evolution of sinuous deep - water channel systems. *Journal of Geophysical Research: Oceans*, 125(3), 1–30. <https://doi.org/10.1029/2019JC015284>
- Dennis, J. E. J. (1977). Nonlinear least squares. In D. Jacobs (Ed.), *The state of the art in numerical analysis* (pp. 269–312). Academic Press.
- Dorrell, R. M., Darby, S. E., Peakall, J., Sumner, E. J., Parsons, D. R., & Wynn, R. B. (2013). Superelevation and overspill control secondary flow dynamics in submarine channels. *Journal of Geophysical Research: Oceans*, 118(8), 3895–3915. <https://doi.org/10.1002/jgrc.20277>
- Dorrell, R. M., Darby, S. E., Peakall, J., Sumner, E. J., Parsons, D. R., & Wynn, R. B. (2014). The critical role of stratification in submarine channels: Implications for channelization and long runout of flows. *Journal of Geophysical Research: Oceans*, 119(4), 2620–2641. <https://doi.org/10.1002/2014JC009807>.Received
- Fildani, A., & Normark, W. R. (2004). Late Quaternary evolution of channel and lobe complexes of Monterey Fan. *Marine Geology*, 206(1–4), 199–223. <https://doi.org/10.1016/j.margeo.2004.03.001>
- Hage, S., Galy, V. V., Cartigny, M. J. B., Acikalin, S., Clare, M. A., Gröcke, D. R., et al. (2020). Efficient preservation of young terrestrial organic carbon in sandy turbidity-current deposits. *Geology*, 48(9), 882–887. <https://doi.org/10.1130/G47320.1>
- Imran, J., Parker, G., & Pirmez, C. (1999). A nonlinear model of flow in meandering submarine and subaerial channels. *Journal of Fluid Mechanics*, 400, 295–331. <https://doi.org/10.1017/S0022112099006515>
- Kane, I. A., McCaffrey, W. D., & Peakall, J. (2008). Controls on sinuosity evolution within submarine channels. *Geology*, 36(4), 287–290. <https://doi.org/10.1130/G24588A.1>
- Khripounoff, A., Vangriesheim, A., Babonneau, N., Crassous, P., Dennielou, B., & Savoye, B. (2003). Direct observation of intense turbidity current activity in the Zaire submarine valley at 4000 m water depth. *Marine Geology*, 194(3–4), 151–158. [https://doi.org/10.1016/S0025-3227\(02\)00677-1](https://doi.org/10.1016/S0025-3227(02)00677-1)
- Klaucke, I. (1995). *The submarine drainage system of the Labrador Sea: Result of glacial input from the Laurentide Ice sheet*. McGill University. McGill University.
- Klaucke, I., Hesse, R., & Ryan, W. B. F. (1997). Flow parameters of turbidity currents in a low-sinuosity giant deep-sea channel. *Sedimentology*, 44(6), 1093–1102. <https://doi.org/10.1111/j.1365-3091.1997.tb02180.x>

- Klaucke, I., Hesse, R., & Ryan, W. B. F. (1998). Seismic stratigraphy of the Northwest Atlantic Mid-Ocean Channel: Growth pattern of a Mid-Ocean channel-levee complex. *Marine and Petroleum Geology*, 15(6), 575–585. [https://doi.org/10.1016/S0264-8172\(98\)00044-0](https://doi.org/10.1016/S0264-8172(98)00044-0)
- Komar, P. D. (1969). The channelized flow of turbidity currents with application to Monterey deep-sea fan channel. *Journal of Geophysical Research*, 74(18), 4544–4558. <https://doi.org/10.1029/jc074i018p04544>
- Konsoer, K., Zinger, J., & Parker, G. (2013). Bankfull hydraulic geometry of submarine channels created by turbidity currents: Relations between bankfull channel characteristics and formative flow discharge. *Journal of Geophysical Research: Earth Surface*, 118(1), 216–228. <https://doi.org/10.1029/2012JF002422>
- Marshall, J. D., Tucker, O. D., & Lovelock, C. E. (2016). Goldeneye: Modelling a depleted field for carbon capture – How much uncertainty is left? *Petroleum Geoscience*, 22(1), 37–45. <https://doi.org/10.1144/petgeo2014-072>
- Mayall, M., Jones, E., & Casey, M. (2006). Turbidite channel reservoirs—Key elements in facies prediction and effective development. *Marine and Petroleum Geology*, 23(8), 821–841. <https://doi.org/10.1016/j.marpetgeo.2006.08.001>
- Migeon, S., Ducassou, E., Le Gonidec, Y., Rouillard, P., Mascle, J., & Revel-Rolland, M. (2010). Lobe construction and sand/mud segregation by turbidity currents and debris flows on the western Nile deep-sea fan (Eastern Mediterranean). *Sedimentary Geology*, 229(3), 124–143. <https://doi.org/10.1016/j.sedgeo.2010.02.011>
- Parker, G., Garcia, M., Fukushima, Y., & Yu, W. (1987). Experiments on turbidity currents over an erodible bed. *Journal of Hydraulic Research*, 25(1), 123–147. <https://doi.org/10.1080/00221688709499292>
- Parsons, D. R., Peakall, J., Aksu, A. E., Flood, R. D., Hiscott, R. N., Beşiktepe, Ş., & Moulard, D. (2010). Gravity-driven flow in a submarine channel bend: Direct field evidence of helical flow reversal. *Geology*, 38(12), 1063–1066. <https://doi.org/10.1130/G31121.1>
- Peakall, J., Amos, K. J., Keevil, G. M., William Bradbury, P., & Gupta, S. (2007). Flow processes and sedimentation in submarine channel bends. *Marine and Petroleum Geology*, 24(6–9), 470–486. <https://doi.org/10.1016/j.marpetgeo.2007.01.008>
- Peakall, J., Kane, I. A., Masson, D. G., Keevil, G., McCaffrey, W., & Corney, R. (2012). Global (latitudinal) variation in submarine channel sinuosity. *Geology*, 40(1), 11–14. <https://doi.org/10.1130/G32295.1>
- Peakall, J., McCaffrey, B., & Kneller, B. (2000). A process model for the evolution, morphology, and architecture of sinuous submarine channels. *Journal of Sedimentary Research*, 70(3), 434–448. <https://doi.org/10.1306/2dc4091c-0e47-11d7-8643000102c1865d>
- Peakall, J., Wells, M. G., Cossu, R., Kane, I. A., Masson, D. G., Keevil, G. M., et al. (2013). Global (latitudinal) variation in submarine channel sinuosity: Reply. *Geology*, 41(5), e288. <https://doi.org/10.1016/j>
- Piper, D. J. W., & Normark, W. R. (2001). Sandy fans from Amazon to huene and beyond. *American Association of Petroleum Geologists Bulletin*, 85(8), 1407–1438. <https://doi.org/10.1306/8626cadc-173b-11d7-8645000102c1865d>
- Pirmez, C., & Flood, R. D. (1995). Morphology and structure of Amazon Channel. *Proceedings of the Ocean Drilling Program, 155 Initial Reports*, 155, 23–45. <https://doi.org/10.2973/odp.proc.ir.155.103.1995>
- Pirmez, C., & Imran, J. (2003). Reconstruction of turbidity currents in Amazon Channel. *Marine and Petroleum Geology*, 20(6–8), 823–849. <https://doi.org/10.1016/j.marpetgeo.2003.03.005>
- Popescu, I., Lericolais, G., Panin, N., Normand, A., Dinu, C., & Le Drezen, E. (2004). The Danube submarine canyon (Black Sea): Morphology and sedimentary processes. *Marine Geology*, 206(1–4), 249–265. <https://doi.org/10.1016/j.margeo.2004.03.003>
- Popescu, I., Lericolais, G., Panin, N., Wong, H. K., & Droz, L. (2001). Late quaternary channel avulsions on the Danube deep-sea fan, black sea. *Marine Geology*, 179(1–2), 25–37. [https://doi.org/10.1016/S0025-3227\(01\)00197-9](https://doi.org/10.1016/S0025-3227(01)00197-9)
- Ren, P., Bornhold, B. D., & Prior, D. B. (1996). Seafloor morphology and sedimentary processes, Knight inlet, British Columbia. *Sedimentary Geology*, 103(3–4), 201–228. [https://doi.org/10.1016/0037-0738\(95\)00090-9](https://doi.org/10.1016/0037-0738(95)00090-9)
- Straub, K. M., & Mohrig, D. (2008). Quantifying the morphology and growth of levees in aggrading submarine channels. *Journal of Geophysical Research*, 113(3), 1–20. <https://doi.org/10.1029/2007JF000896>
- Straub, K. M., Mohrig, D., McElroy, B., Buttles, J., & Pirmez, C. (2008). Interactions between turbidity currents and topography in aggrading sinuous submarine channels: A laboratory study. *Bulletin of the Geological Society of America*, 120(3–4), 368–385. <https://doi.org/10.1130/B25983.1>
- Sumner, E. J., & Paull, C. K. (2014). Swept away by a turbidity current in Mendocino submarine canyon, California. *Geophysical Research Letters*, 41(21), 7611–7618. <https://doi.org/10.1002/2014GL061863>
- Sumner, E. J., Peakall, J., Dorrell, R. M., Parsons, D. R., Darby, S. E., Wynn, R. B., et al. (2014). Driven around the bend: Spatial evolution and controls on the orientation of helical bend flow in a natural submarine gravity current. *Journal of Geophysical Research: Oceans*, 119(2), 898–913. <https://doi.org/10.1002/2013JC009563>
- Sylvester, Z., & Pirmez, C. (2019). Latitudinal changes in the morphology of submarine channels: Reevaluating the evidence for the influence of the coriolis force. *SEPM Special Publications*, 108, 82–92. <https://doi.org/10.2110/sepm.108.02>
- Sylvester, Z., Pirmez, C., Cantelli, A., & Jobe, Z. R. (2013). Global (latitudinal) variation in submarine channel sinuosity: Comment. *Geology*, 41(5), e287. <https://doi.org/10.1130/G33548C.1>
- Talling, P. J., Masson, D. G., Sumner, E. J., & Malgesini, G. (2012). Subaqueous sediment density flows: Depositional processes and deposit types. *Sedimentology*, 59(7), 1937–2003. <https://doi.org/10.1111/j.1365-3091.2012.01353.x>
- Torres, J., Droz, L., Savoye, B., Terentjeva, E., Cochonat, P., Kenyon, N. H., & Canals, M. (1997). Deep-sea avulsion and morphosedimentary evolution of the Rhône fan valley and Neofan during the late Quaternary (north-western Mediterranean sea). *Sedimentology*, 44(3), 457–477. <https://doi.org/10.1046/j.1365-3091.1997.d01-36.x>
- Vangriesheim, A., Khripounoff, A., & Crassous, P. (2009). Turbidity events observed in situ along the Congo submarine channel. *Deep-Sea Research Part II Topical Studies in Oceanography*, 56(23), 2208–2222. <https://doi.org/10.1016/j.dsr2.2009.04.004>
- Wells, M. G., & Cossu, R. (2013). The possible role of Coriolis forces in structuring large-scale sinuous patterns of submarine channel – Levee systems. *Philosophical Transactions of the Royal Society A*, 371(2004), 1–19. <https://doi.org/10.1098/rsta.2012.0366>
- Wells, M. G., & Dorrell, R. M. (2021). Turbulence processes within turbidity currents. *Annual Review of Fluid Mechanics*, 53(1), 59–83. <https://doi.org/10.1146/annurev-fluid-010719-060309>
- Wynn, R. B., Cronin, B. T., & Peakall, J. (2007). Sinuous deep-water channels: Genesis, geometry and architecture. *Marine and Petroleum Geology*, 24(6–9), 341–387. <https://doi.org/10.1016/j.marpetgeo.2007.06.001>
- Xu, J. P., Sequeiros, O. E., & Noble, M. A. (2014). Sediment concentrations, flow conditions, and downstream evolution of two turbidity currents, Monterey Canyon, USA. *Deep-Sea Research Part I Oceanographic Research Papers*, 89, 11–34. <https://doi.org/10.1016/j.dsr.2014.04.001>
- Zhong, G., & Peng, X. (2021). Transport and accumulation of plastic litter in submarine canyons—The role of gravity flows. *Geology*, 49(5), 581–586. <https://doi.org/10.1130/G48536.1>